AGU PUBLICATIONS

JGR

Journal of Geophysical Research: Oceans

RESEARCH ARTICLE

10.1002/2014JC010490

Impact of multichannel river network on the plume dynamics in the Pearl River estuary

Zhigang Lai[1,2], Ronghua Ma[1], Guangyin Gao[1], Changsheng Chen[3,4], and Robert C. Beardsley[5]

[1]School of Marine Sciences, Sun Yat-Sen University, Guangzhou, China, [2]Key Laboratory of Marine Resources and Coastal Engineering in Guangdong Province, Guangzhou, China, [3]School for Marine Science and Technology, University of Massachusetts-Dartmouth, New Bedford, Massachusetts, USA, [4]International Center for Marine Studies, Shanghai Ocean University, Shanghai, China, [5]Department of Physical Oceanography, Woods Hole Oceanographic Institution, Woods Hole, Massachusetts, USA

Key Points:
- The discharge plume is a key feature of the Pearl River plume in the dry season
- The river network and estuary interaction controls the discharge plume dynamics
- Resolving the QiAo Channel is critical to capture the Pearl River plume

Correspondence to:
Z. Lai,
laizhig@mail.sysu.edu.cn

Citation:
Lai, Z., R. Ma, G. Gao, C. Chen, and R. C. Beardsley (2015), Impact of multichannel river network on the plume dynamics in the Pearl River estuary, *J. Geophys. Res. Oceans*, *120*, 5766–5789, doi:10.1002/2014JC010490.

Received 6 OCT 2014
Accepted 29 JUL 2015
Accepted article online 1 AUG 2015
Published online 21 AUG 2015

Abstract Impacts of the multichannel river network on plume dynamics in the Pearl River estuary were examined using a high-resolution 3-D circulation model. The results showed that during the dry season the plume was a distinct feature along the western coast of the estuary. The plume was defined as three water masses: (a) riverine water (<5 psu), (b) estuarine water (12–20 psu), and (c) diluted water (>22 psu), respectively. A significant amount of low-salinity water from Hengmen and Hongqimen was transported through a narrow channel between the QiAo Island and the mainland of the Pearl River delta during the ebb tide and formed a local salinity-gradient feature (hereafter referred to as a discharge plume). This discharge plume was a typical small-scale river plume with a Kelvin number $K = 0.24$ and a strong frontal boundary on its offshore side. With evidence of a significant impact on the distribution and variability of the salinity and flow over the West Shoal, this plume was thought to be a major feature of the Pearl River plume during the dry season. The upstream multichannel river network not only were the freshwater discharge sources but also played a role in establishing an estuarine-scale subtidal pressure gradient. This pressure gradient was one of the key dynamical processes controlling the water exchange between discharge and river plumes in the Pearl River estuary. This study clearly showed the role of the river network and estuary interaction on river plume dynamics.

1. Introduction

River plumes in estuaries or bays generally behave in a manner featured by an anticyclonic turning outflow and alongshelf currents (in the Northern Hemisphere) with the formation of a recirculating bulge in the advective convergence zones off the mouth of the river [*Chao and Boicourt*, 1986; *Kourafalou et al*., 1996; *Chen et al*., 1999; *Yankovsky*, 2000; *Nof and Pichevin*, 2001]. The structure, mixing, transport, and variability of a river plume over the inner shelf are often significantly influenced or even controlled by the wind stress and ambient currents [*Chao*, 1988; *Chen*, 2000; *Fong and Geyer*, 2001, 2002; *Garcia Berdeal et al*., 2002; *Whitney and Garvine*, 2005; *Choi and Wilkin*, 2007; *de Boer et al*., 2007; *Otero et al*., 2008; *Hetland*, 2005, 2010]. In addition to our current understanding, the dynamics controlling a river plume, particularly within an estuary, can be highly complex, with features of rough bathymetry and multiple forcing variables [*MacCready and Geyer*, 2010]. This can make the water and salt exchanges more vigorous and strongly nonlinear within an estuary than over the shelf, with the physical processes covering a wide range of time scale [*Halverson and Pawlowicz*, 2008]. So, river plumes in estuaries may include physical processes that are often ignored by previous studies of coastal plume discharge. Particularly, in a tidal river-estuary system, the river plays an important role in energy and mass balances by storage of tidal water during the flood tide and persistent dissipation of tidal energy. This process, in turn, affects the energy and mass distribution of the estuary where the river plume is a dominant physical feature. Moreover, if the estuary is connected with a multichannel river network, the differential interaction of individual channels with the estuary can produce an even complex estuarine dynamics, which may be crucial for the underlying features of the river plume.

The Pearl River estuary (PRE) is located at the northern reach of the South China Sea (SCS). It is bell-shaped in horizontal view, with a major axis of ~70 km in the north-south direction and a width increasing from ~15 km at the northern end to ~35 km at its mouth (Figure 1). The PRE includes three shoals (West Shoal,

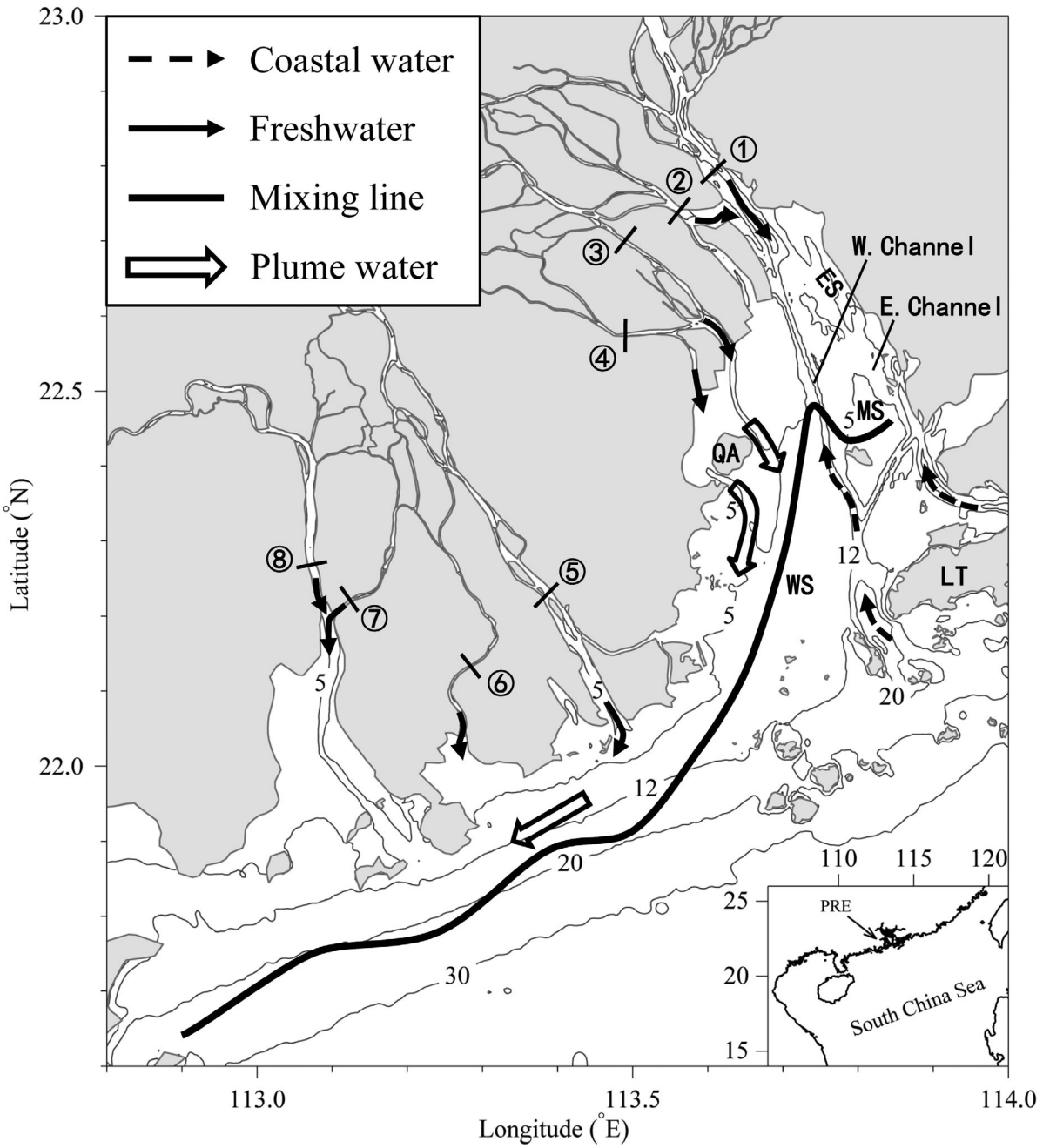

Figure 1. Map of location and bathymetry of the Pearl River Estuary. The river plume in the PRE and adjacent coastal area during the dry season is indicated. The circled numbers represent the eight river outlets of the Pearl River that are Humen, Jiaomen, Hongqimen, Hengmen, Modaomen, Jitimen, Hutiaomen and Yamen, respectively, from ①-⑧. The abbreviations LT, QA, WS, MS, and ES mean Lantou Island, QiAo Island, West Shoal, Middle Shoal, and East Shoal, respectively.

Middle Shoal, and East Shoal) and two longitudinal deep channels (West Channel and East Channel). The averaged depth of the PRE is only ~5 m, with the bathymetry varying between 10 and 20 m in the deep channels. To the north and west of the PRE is a delta, where river runoff from the Pearl River, one of the most complex-structured river systems in the world, flows in through eight outlets (called gates in Chinese). These are Humen, Jiaomen, Hongqimen, Hengmen, Modaomen, Jitimen, Hutiaomen, and Yamen, respectively, from east to west.

The key physical processes of the PRE are mainly tides, river discharge, and winds. The mean tidal range is 1.0 m outside the mouth of the estuary and increases to 1.7 m in the upstream region. The mean residual current is counterclockwise with a stronger flood tidal flow on the east side of the estuary and a stronger

ebb tidal flow on the west side of the estuary [*Mao et al*., 2004]. The freshwater discharge of the Pearl River varies seasonably, with about 80% of the annual discharge occurring in the wet season from April to September and only 20% occurring in the dry season from October to March [*Zhao*, 1990]. The wind in this region is seasonally reversed with the northeasterly monsoon in winter and the southwesterly monsoon in summer. The outflow of the Pearl River forms multiple shallow, buoyant freshwater plumes, which have a direct influence on the estuarine circulation and coastal ecological environment in the PRE and adjacent coastal area [*Harrison et al*., 2008].

The dynamics of the Pearl River plume are influenced by many physical factors such as river discharge, bathymetry, tides, wind stress, and turbulent mixing. In summer, the surface area of the PRE is entirely occupied by the plume water. The salinity inside the estuary is usually <5 and is about 5–9 near the mouth [*Dong et al*., 2004]. The size of the plume (measured with a boundary on the 32 isohaline) is much larger than the area of the estuary, so that mixing of the plume water with ambient coastal water mainly occurs outside the estuary. The evolution of the plume is controlled by several factors including river discharge, winds, and inshore sea surface height [*Xue and Chai*, 2001]. Among these, the monthly river discharge rate is highly related with the size and shape of the plume with a correlation coefficient up to 0.85 [*Ou et al*., 2009], while the spreading path of the plume is driven by winds and can be categorized into four types that are named "Offshore Bulge Spreading, West Alongshore Spreading, East Offshore Spreading, and Symmetrical Alongshore Spreading" [*Ou et al*., 2009]. In the winter dry season, the plume only appears at the western part of the estuary as a result of the reduced river discharge and the prevailing northeasterly monsoon [*Ying and Chen*, 1983; *Ji et al*., 2011]. In turn, the coastal water intrudes into the east part of the estuary through the West and East Channels [*Dong et al*., 1985; *Yang et al*., 1995], forming a large salinity gradient in the PRE that runs from the northwest with riverine water to the southeast with more saline coastal waters [*Xu et al*., 1981].

A number of theoretical and numerical modeling studies have been conducted to examine the plume dynamics in the PRE and adjacent coastal regions. Among them, the summer plume was intensively investigated in many details. The research was mainly focused on the interaction of the plume water with the wind-driven coastal processes, such as the role of winds on the plume's horizontal spreading pattern [*Ou et al*., 2009], the interaction of the plume with the summer monsoon-driven upwelling circulations [*Gan et al*., 2009; *Shu et al*., 2011], and the response of the plume anatomy and frontal properties to wind forcing [*Pan et al*., 2014]. The research on the winter plume, however, was mainly focused on the dynamics of the plume front within the PRE. For example, *Wong et al*., [2004] used a numerical model to simulate the surface and bottom fronts of the plume in the PRE during the dry season and reported that the structure and variability of these fronts were highly related with the variation of estuarine processes such as tides, river discharge, and winds. The southwestward coastal current outside the PRE was also important for the plume close to the mouth of the estuary which constrained the plume to the west side of the estuary and formed a sharp salinity front [*Ji et al*., 2011]. Recently, a sensitivity study on the winter plume front suggested that the location of the front was sensitive to the amount of discharge given at each outlet of the river [*Zheng et al*., 2014]. This was an interesting finding because it implied that both the Pearl River and the estuary may be critical in terms of plume dynamics. Since the winter plume evolved under complex conditions within the estuary, many details of the plume dynamics still remain unclear.

In particular, what is the role of the river network in determining the plume structure and variability in the PRE? This question, which is potentially important for the dynamics of the winter plume, has not been investigated in previous studies. It is clear that the Pearl River is a complex multichannel river system with many intersections and bifurcations. The upstream river runoff is discharged into the estuary by distributing its volume transport through eight river outlets. Due to nonlinear interaction between the river and the estuary, the freshwater discharge at the river outlet is a complex function of the upstream inflow, tides, and estuarine circulation as well as the structure of the river network. According to previous finding that the winter plume front in the PRE was very sensitive to the amount of discharge given at each outlet [*Zheng et al*., 2014], the river inflow condition in the model could be a critical factor to determine the plume structure and even its variability. If that is the case, ideally it requires the river and estuary to be integrated in the model, with the river boundaries being moved to farther upstream locations where only the influence from the river is considered. However, in previous numerical simulations, the Pearl River is either simplified as several single-cell-wide straight channels or simply removed by specifying the inflow conditions at the

locations of the river outlets. By giving the proportion of the river discharge rate at individual outlets, the model with these types of model configuration reasonably captured general features of the river plume as well as the plume front [*Larson et al*., 2005; *Hu and Li*, 2009]. However, no study has examined the sensitivity of the model results to such simple treatments of the river network and dynamics controlling the water exchange between the outlets and estuary. Therefore, it raises the question whether a model that includes the realistic geometry of the Pearl River is necessary to capture the plume dynamics in the dry season?

In this paper, the main purpose aims at identifying the critical roles of the river network in the river plume in the PRE during the dry season. Results gained from this study could be applied for modeling researches in many other estuaries where the dynamics is controlled by a multichannel river system and small-scale features of the local geometry or bathymetry. The numerical experiments conducted in this study were focused on the essential dynamical processes instead of demonstrating how accurate the simulation were. The remainder of this paper is organized as follows. In section 2, the model setup and designs of numerical experiments are described. In section 3, the validation results are presented, followed by a detailed description of the model-predicted river plume in section 4. The findings are discussed in section 5 and conclusions are summarized in section 6.

2. Material and Methods

A river-estuary-integrated 3-D PRE circulation model (hereafter referred to as PRE-FVCOM) was established based on the primitive equations, unstructured-grid, Finite-Volume Community Ocean Model (FVCOM). FVCOM is developed originally by *Chen et al*. [2003] and continuously improved and updated by the joint research team of University of Massachusetts-Dartmouth and Woods Hole Oceanographic Institution [*Chen et al*., 2006a, 2006b, 2013]. The model had a domain covering the Pearl River with all its tributaries: West River, North River, East River, Liuxi River, Zeng River, and Tan River, the estuary, and the shelf of the northern SCS to the 100 m isobath along the Guangdong coast (Figure 2a). This large model domain ensured that the spreading of the river plume would not be affected by the forcing uncertainties at the open boundary. Horizontally, the model had a grid size varying from $\sim$20 to 300 m within the Pearl River, 100–500 m in the PRE and adjacent area, and $\sim$500 m nearshore to $\sim$10 km at the most southern open boundary. In the nearshore region along the western shoreline of the PRE, the grid size was specified to be 100 m in order to resolve the detailed structure of the river plume and the front. Vertically, a hybrid terrain-following coordinate was used, which had a total of 45 layers and a coordinate transition at the 225 m isobath. In the region with the depth of $>$225 m, the s-coordinate was adopted; otherwise the σ-coordinate with uniform layer thickness in the vertical was applied. Since the average depth of the PRE was $\sim$5 m, this setup created an averaged layer thickness of about 0.1 m in the PRE, which was high enough to resolve the vertical circulation within the river plume.

The numerical experiments covered the period from 1 November to 31 December 2011. The PRE-FVCOM was driven by tidal forcing at the open boundary, river discharges from the upstream end, and atmospheric forcing at the surface. It was initialized with November climatology of the T/S field and spun up from zero velocity and undisturbed sea surface elevation. In the estuarine and shelf regions, the initial climatology T/S was obtained from the database that was used to initialize the China coastal FVCOM [*Chen et al*., 2012]. In the river network, the initial temperature was set as the same as in the estuary while the initial salinity was set as zero with a transition distance to the estuary following *Zu et al*. [2007].

There were two types of river discharge data used in the model. For the three largest tributaries of the Pearl River including the West River, the North River, and the East River, hourly data were specified based on observations made at hydrological stations at Gaoyao, Shijiao, and Boluo, respectively (Figure 2a). For other small rivers including the Liuxi River, the Zeng River, and the Tan River, climatologically monthly mean data were specified at hydrological stations at Laoyagang, Qilinzui, and Shizui, respectively. Figure 3 shows the time series of the hourly total river discharge specified in the model during the study period. The hourly discharges exhibited a generally decreasing trend with a mean value of 2276 m^3/s, which only accounted for 15% of the annually mean river discharge. In addition to specifying freshwater discharges at river boundary, salinity and temperature values were also required. We simply set the salinity to be 0 and the temperature to be a constant value of 15°C for the river inflow. These values represented typical conditions of water

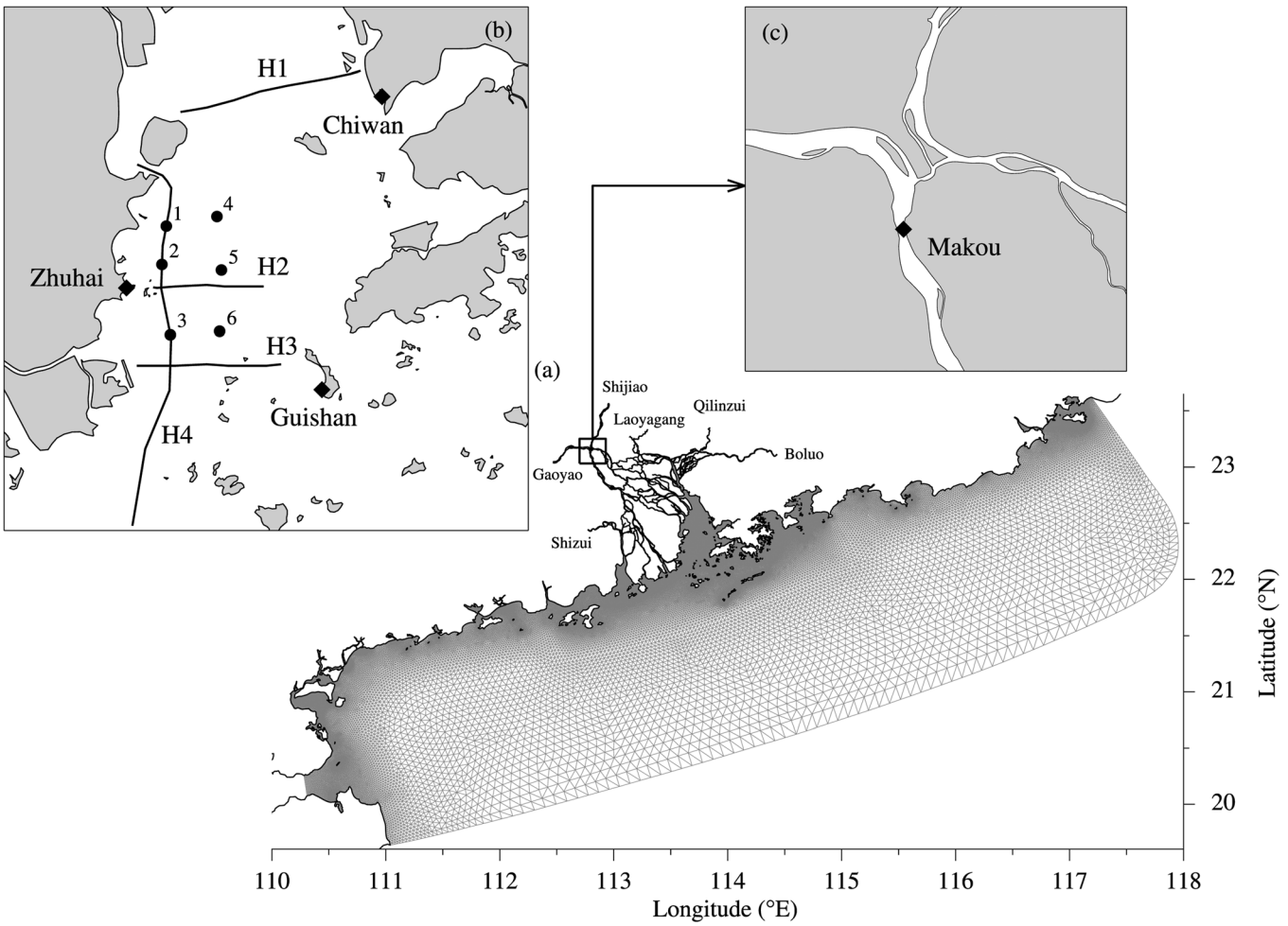

Figure 2. (a) Model domain shown by the surface meshes in which the names of the hydrological stations located at the model's river boundary of the six major tributaries of the Pearl River are indicated; (b) Location of the tidal gauges in Figure 4 and the locations of the cross sections for model validation with observation data adopted from *Dong et al*. [2004]. Labels 1–6 are the six sampling stations listed in Figure 19; and (c) Enlarged view of the location of the tidal gauge Makou.

salinity and temperature in the upstream end of the river for this season. At open boundaries, a tracer radiation condition was specified.

The tidal forcing at the open boundary was specified using the model-predicted real-time sea surface heights constructed using the amplitudes and phases of eight major tidal constituents (four semidiurnal: M_2, S_2, N_2, and K_2, and four diurnal: K_1, P_1, O_1, Q_1) [*Pawlowicz et al*., 2002]. These tidal constituents specified at the open boundary were produced by the tidal simulation using the China coastal FVCOM and validated by the comparison with the sea level data recorded at available tidal gauges along China's coast [*Chen et al*., 2012].

The surface forcing was from a 4 km resolution WRF (Weather Research and Forecast) mesoscale weather model output over the PRE and coastal regions. During the simulation period, the winds in the study period were primarily in the easterly-northeasterly direction with an average speed of ~6.0 m/s. As shown in Figure 3, the wind varied significantly in both direction and speed in November, and then stayed in the southwestward direction in December. Our studies were focused on the variability of river discharge induced plume that is featured by salinity. To avoid error in the SST simulation due to the inaccurate WRF-calculated shortwave irradiance at the surface, a daily SST product with a 1 km resolution downloaded from (http://podaac.jpl.nasa.gov/dataset/JPL_OUROCEAN-L4UH_fnd-GLOB-G1SST) was assimilated into the model to adjust the model-computed daily mean of the SST. A reasonable good agreement was found between model-predicted and observed hourly sea surface temperatures at surveying time, indicating that the model run with the daily SST adjustment was capable of reproducing the estuary SST pattern under good weather conditions in December 2011.

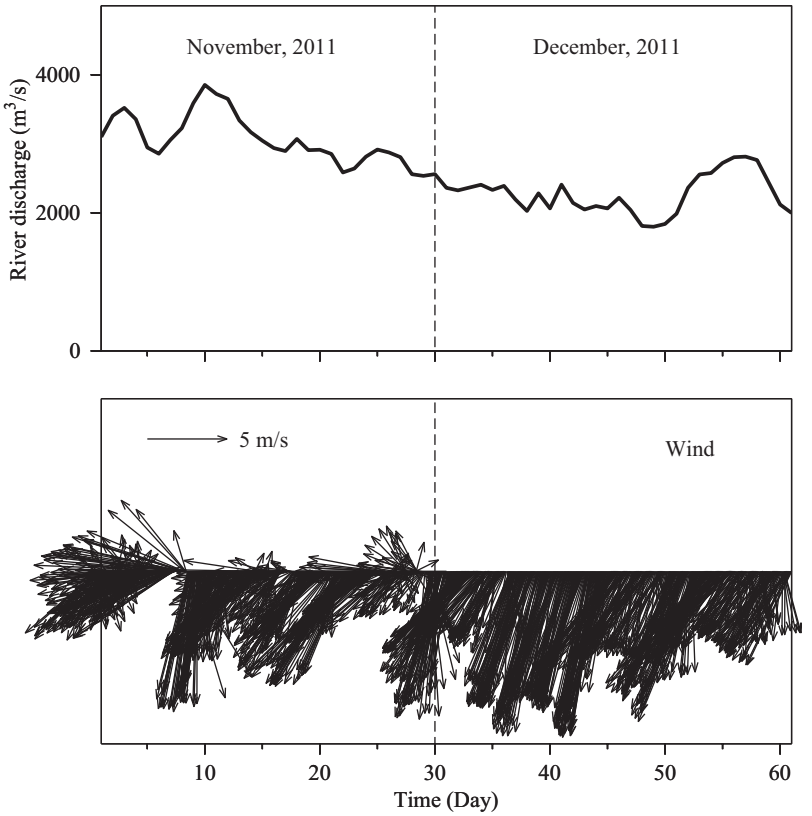

Figure 3. (top) Time series of the hourly total river discharge used in the model; (bottom) Time series of the wind data used in the model.

The time integration of the model used the split-mode time stepping method with a 1 s external time step and a split number of 5. The wet/dry treatment was turned on because part of the upstream river channels had a bottom depth above the mean sea level. The vertical eddy viscosity and horizontal diffusion coefficients used in the model were calculated using the Mellor and Yamada level 2.5 (MY-2.5) [*Mellor and Yamada*, 1982] and Smagorinsky [*Smagorinsky*, 1963] turbulent closure schemes, respectively. The model was spun up for tidal forcing over the first 5 days, and then run continuously with the inclusion of all forcings through November and December. The model-predicted river plume reached a quasi-equilibrium state in late November, and the hourly model output in December was used for analysis.

3. Model Validation

3.1. Tides

The tidal constituents at the open boundary were validated by comparing the amplitudes and phase lags of the model-computed tidal elevation with those at tidal gauges along the coasts of the PRE. An example of the model data differences for the dominant semidiurnal tide M_2 and the diurnal tide K_1 at each station is given in Table 1 and the summary of the results for other constituents is given in Table 2. Generally, the model results were in good agreement with the observations. The amplitudes and phase lags of the mean absolute difference for all constituents were less than 4 cm and 6°, respectively; while the correspondingly mean RMS errors were less than 5 cm and 8°, respectively. In addition, the time series of model-computed and observed water-levels at hydrological stations of Makou in the Pearl River network and Chiwan, Guishan, and Zhuhai in the PRE (see Figures 2b–2c for locations) over the period of December 2011 are shown in Figure 4. The results showed that the model not only predicted the tidal variation in the estuary well but also the tidal deformation in the course of propagation into the river. The model-data comparisons demonstrated that the model was capable of reproducing the tidal process in the PRE, which was critical for the analysis of tidal-scale variability of the river plume.

Table 1. Comparison Between Computed and Observed M_2 and K_1 Tides in the PRE and Adjacent Coastal Area[a]

				M_2			K_1		
No.	Site	Longitude (E)	Latitude (N)	H (cm)	$\triangle H$ (cm)	$\triangle g$ (°)	H (cm)	$\triangle H$ (cm)	$\triangle g$ (°)
1	Xiachuan	112°32.0′	22°37.0′	60.0	−4.8	3.3	40.0	−1.4	−9.7
2	Sanzhao	113°25.1′	22°2.0′	45.8	−1.8	−1.9	35.9	0.5	1.4
3	Dahengqin	113°29.0′	22°5.0′	43.0	−2.0	1.7	35.0	−0.5	2.8
4	Macau	113°33.0′	22°11.0′	54.0	−9.5	17.7	41.0	−4.2	13.4
5	Zhuhai	113°33.0′	22°11.0′	51.4	−6.2	3.0	48.4	−11.3	−1.9
6	Nansha	113°34.5′	22°43.5′	49.7	3.3	−4.2	31.0	7.2	0.0
7	Shajiao	113°39.3′	22°45.1′	63.6	−8.6	6.4	45.7	−6	−4.3
8	Neilingding	113°48.0′	22°25.0′	56.5	−7.3	0.0	38.5	−0.3	5.0
9	Chiwan	113°52.9′	22°27.4′	59.8	−8.5	0.9	39.2	−0.4	7.0
10	Dawanshan	113°43.0′	21°56.0′	40.5	0.2	0.1	36.6	−0.9	−7.2
11	Wenweizhou	113°56.0′	21°49.0′	30.0	6.7	−5.1	33.0	1.6	−0.2
12	Wailingding	114°2.0′	22°6.0′	41.0	−2.6	−3.2	35.0	0.1	0.1
13	Tai′O	113°51.0′	22°15.0′	53.9	−6.3	−2.8	40.3	−2.7	1.5
14	Shek Pik	113°53.0′	22°13.0′	43.6	−0.5	0.6	36.4	−0.1	1.5
15	Tai Mo To	113°58.0′	22°20.0′	49.0	−3.2	−4.0	40.0	−2.8	−5.6
16	Lok On Pai	114°0.0′	22°22.0′	48.3	−3.5	−5.6	38.3	−1.5	2.1
17	Chi Ma Wan	114°0.0′	22°14.0′	42.4	−2.4	1.7	36.0	−0.5	2.2
18	Hong Kong	114°10.0′	22°18.0′	38.0	1.6	3.9	36.0	−0.6	3.7
19	Quarry Bay	114°13.0′	22°18.0′	39.7	−1.8	−1.4	35.8	−1.0	0.2
20	Dangan Dao	114°7.7′	22°7.3′	33.2	4.1	12.8	23.8	10.9	−9.5
21	Wagland Island	114°18.0′	22°11.0′	33.5	0.9	−2.8	34.2	−0.4	−1.9
22	Tai Po Kau	114°11.0′	22°27.0′	36.1	0.0	−20.7	35.2	−1.0	−9.9
23	Ko Lau Wan	114°21.0′	22°27.0′	34.4	0.3	−1.8	34.1	−0.2	0.0
24	Tuoning Leidao	114°38.0′	22°27.0′	39.0	−7.4	−1.2	34.0	−1.0	−0.8
25	Sanmen Dao	114°38.3′	22°28.2′	30.6	1.1	0.1	33.4	−0.4	2.5
26	Dayawan1	114°32.0′	22°36.0′	33.6	−0.5	−0.8	34.5	−1.1	3.4
27	Tsang Chau	114°44.0′	22°44.0′	37.0	−2.5	2.5	34.0	−0.2	1.7
28	Dayawan2	114°54.0′	22°34.0′	28.9	1.0	−3.3	32.9	−0.4	0.7
	Mean absolute differences				3.5	4.1		2.1	3.6
	RMS				4.0	6.4		3.6	5.0

[a]Note that H is observed tidal amplitude and $\triangle H$, $\triangle g$ are the difference between the model-computed tidal amplitude and phase and the observed tidal amplitude and phase.

3.2. River Plume

The spatial distribution and temporal variation of the simulated river plume were validated by overlapping the model-predicted surface salinity with the satellite-derived sea surface temperature (SST) images collected during December 2011. This comparison was made based on the observational evidence that during the winter the river plume had a similar horizontal distribution pattern as the thermal structure because the river temperature was relatively colder than the water in the estuary [*Tian*, 1994]. This comparison did show that the spatial distribution of the model-predicted river plume was very similar to the spatial structure of the observed SST (Figure 5). Specifically, the model successfully predicted the westward flow of the river plume with a cross-shelf scale matching the zone of cold water. The intrusion of coastal water through the West Channel and East Channel was also evident. It was manifested as a tongue of warm/saline water extending toward the land in the upper estuary. As a result, the temperature and salinity contours coincided each other in the intrusion region. Since the satellite images were made in consecutive days, this comparison suggested that the model was capable of simulating realistically the tidal-scale spatial and temporal variations of the river plume. The matching between salinity and temperature patterns of the river plume assured us of the general soundness of the model's performance. Due to the different natures of

Table 2. Summary of the Tidal Comparison for Other Constituents in the PRE and Adjacent Coastal Area

	Semidiurnal						Diurnal					
	S_2		N_2		K_2		P_1		O_1		Q_1	
	H (cm)	g (°)	H (cm)	g (°)	H (cm)	g (°)	H (cm)	g (°)	H (cm)	g (°)	H (cm)	g (°)
Mean absolute difference	2.3	4.7	0.8	5.2	0.5	5.7	0.7	3.3	1.2	4.7	0.2	3.2
RMS	2.1	7.1	1.2	7.2	0.3	7.8	0.7	4.8	1.7	5.0	0.2	3.8

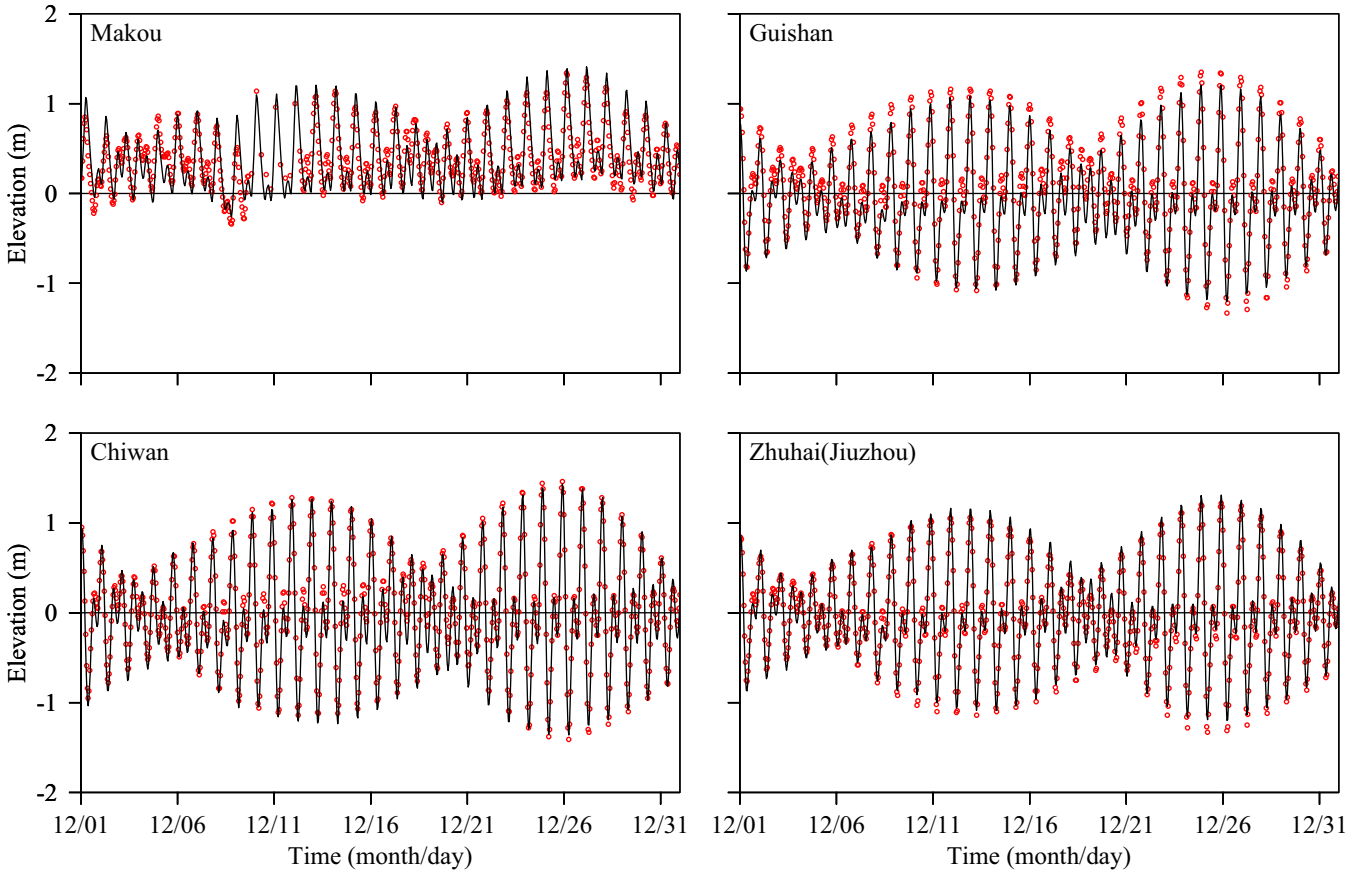

Figure 4. Comparisons between model-computed and observed time series of the tidal elevation over 1–31 December 2011.

temperature and salinity structures in the plume, however, it was still necessary to conduct a further validation of the plume with salinity measurements.

Dong et al. [2004] reported a comprehensive field survey of the river plume in the PRE. The resulting data set was used for our model validations. In Figure 6, we compared the cross-estuarine structure of the observed and model-computed river plumes on three transects as shown in Figure 2b. The observed data used in this comparison were collected over a period from the neap tide to the spring tide during 17–24 January 2000 [*Dong et al.*, 2004]. On transect H1, the data showed that a salinity front was located at the offshore edge of a local topographic channel (Figure 6a). This was evident in the model-computed salinity field, which exhibited a similar salinity difference (Figure 6d). On the right side of the front, there was an isolated band of high-salinity water close to the bottom defined by the 28 isohaline. This implied a possible intrusion of coastal water from the West Channel. In contrast, the model-predicted intrusion looked stronger as the high-salinity water expanded out of the Channel and onto the shelf. On transect H2, the observation revealed an alongshore plume which was subject to substantial mixing and was weakly stratified (Figure 6b). The model-predicted plume exhibited the same spatial pattern as the observation, but it was horizontally more diffused on the offshore side (Figure 6e). Finally, on transect H3, a surface-bottom salinity front, which formed as the boundary of inshore plume water and offshore coastal water and remained weakly stratified in the vertical, was observed at the mouth of the estuary (Figure 6c). This front was reasonably reproduced by the model with a bias that showed that the model-predicted frontal position looked closer to the shore (Figure 6f). The model-data deviation appeared in this comparison was understandable since the observations were not made as the same time as the model simulation. The biases could have resulted from differences in forcing factors such as river discharge and winds. These biases, however, did not affect the objective of this study, because the general features predicted by the model and observed by the field surveys remained the same.

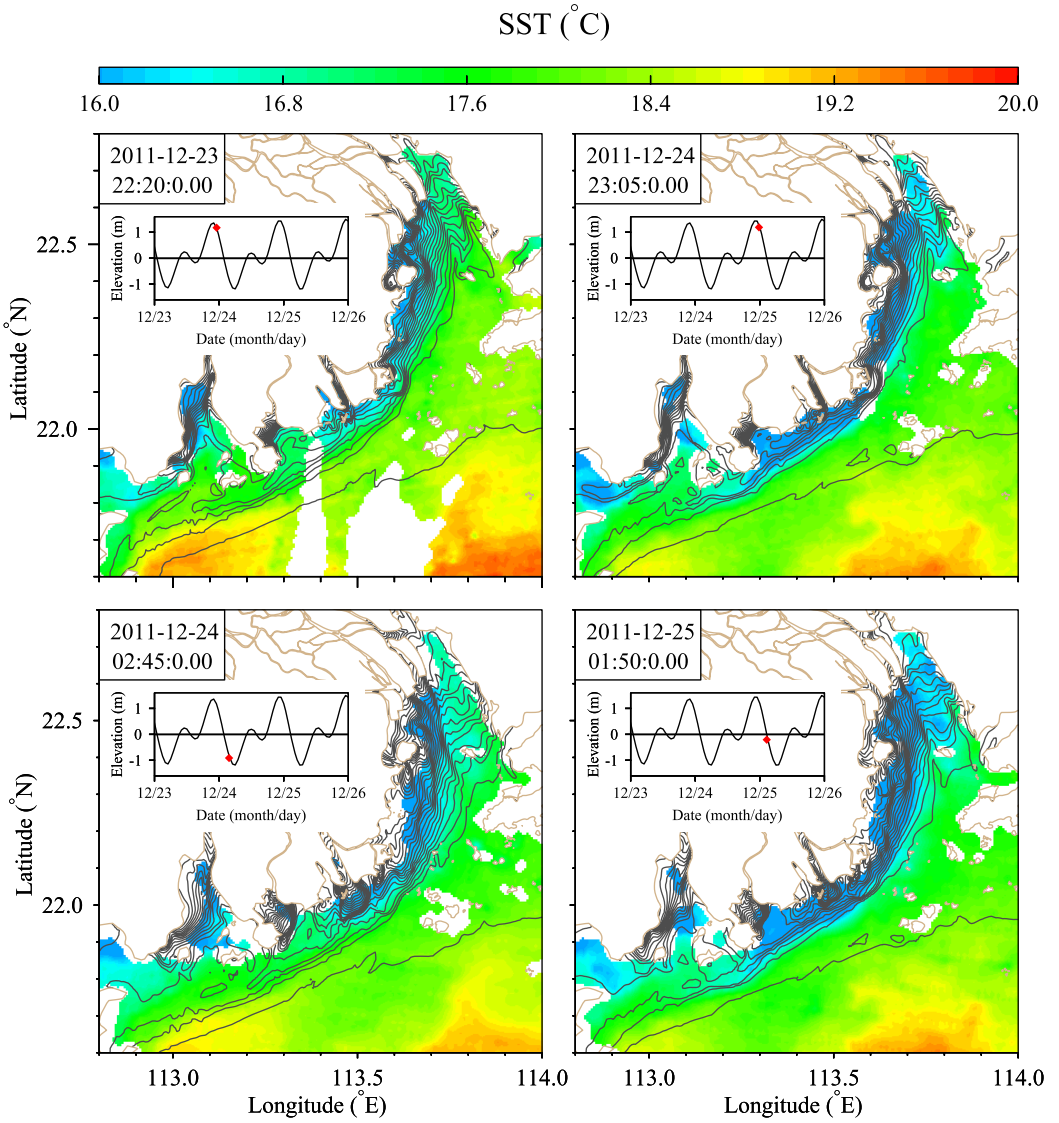

Figure 5. MODIS satellite-derived SST images overlapped with the model-predicted surface salinity in the PRE and adjacent region on 23–25 December 2011. The tidal phases during the observations are indicated correspondingly. Please note that the interval of the salinity contours is 1 and the contour line at the southernmost position represents 34.

4. Results

4.1. Pearl River Plume in the Dry Season

The model results show that during the dry season a buoyant plume forms as a result of the Pearl River discharges from the river network outlets. This plume appeared along the western coast of the estuary, with a surface salinity structure that was most evident during the ebb tidal period (Figure 7). Three types of plume water masses were identified. The freshest plume was located in the region close to the river outlets around the Hongqimen and Hengmen. This plume contained riverine-type water which often had a salinity of <5. The driving mechanism for this plume was mainly associated with freshwater discharge. In the region of this plume, the tidal advection and mixing effects were overwhelmed by buoyancy input. Away from the river outlets, the other two water masses were roughly parallel with each other along the western shoreline. A sharp salinity front appeared on the western coast at the transition from flood tide to ebb tide, which ran southwestward along the shoreline (Figure 7a). This front was defined as an estuarine front in the PRE. On the inshore side of the front, the salinity was in the range of $\sim$12–20. The water was originally from the riverine plume in the upstream estuarine region and significant mixing occurred to overcome the initial buoyance input as it was advected seaward. On the offshore side of this front, there involved a further mixing of

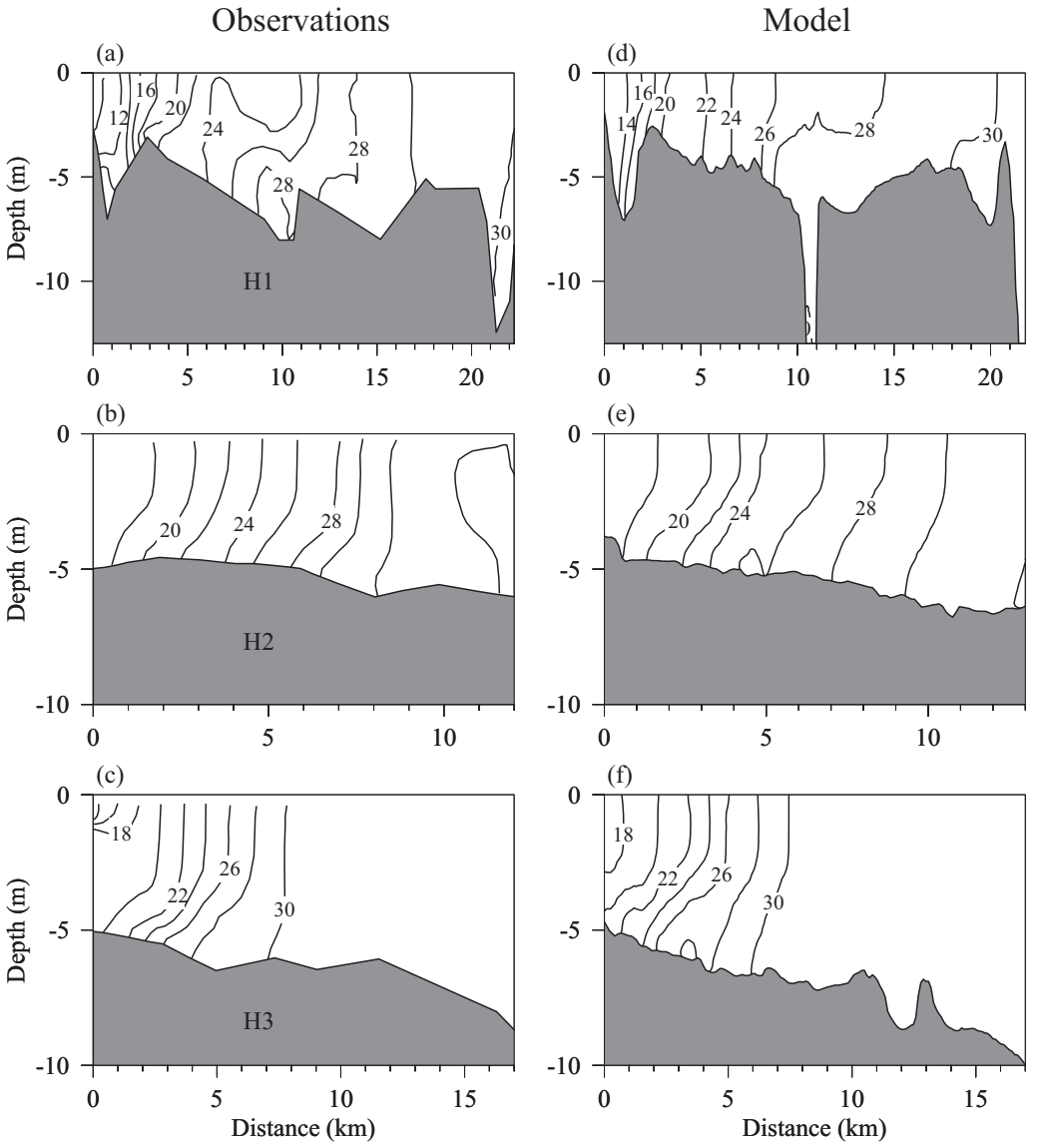

Figure 6. Comparisons of model-computed and observed salinities along the three cross-estuarine transects indicated in Figure 2b on 05:00:00 GMT, 12 December 2011. The observation data were adopted from *Dong et al.* [2004].

the plume water with the ambient coastal water. As a result, a saltier diluted water mass zone with salinity of $>$22 formed parallel to the estuarine front in the PRE.

Winds and tides were the major forcing factors to control the spatial/temporal variability of the Pearl River plume. With only northeast wind, the downwelling-favorable wind tended to push the water against the western coast and form a narrow plume with a relatively stable salinity structure along the western shore (results not shown). In contrast, tides can dam/release freshwater from the rivers periodically, which directly affected the offshore spreading of the plume water and made it vary strongly over tidal cycles (Figure 7). Specifically, during the ebb tidal period, the river discharge plus tidal flow enhanced the outspreading of the riverine plume along the western coast of the estuary and hence pushed the nearshore estuarine water away in the offshore direction. In this course, the estuarine water was subject to substantial mixing and gradually dispersed into the diluted water. During the flood tidal period, the tidal flow caused a retreat of the riverine water toward the river mouth, enabling the estuarine water to be reestablished along the western coast. This water was the remnant of the riverine water released over previous tidal cycles. Since the mixing time scale was relatively shorter, this water was fresher than the offshore diluted water and featured a sharp estuarine front.

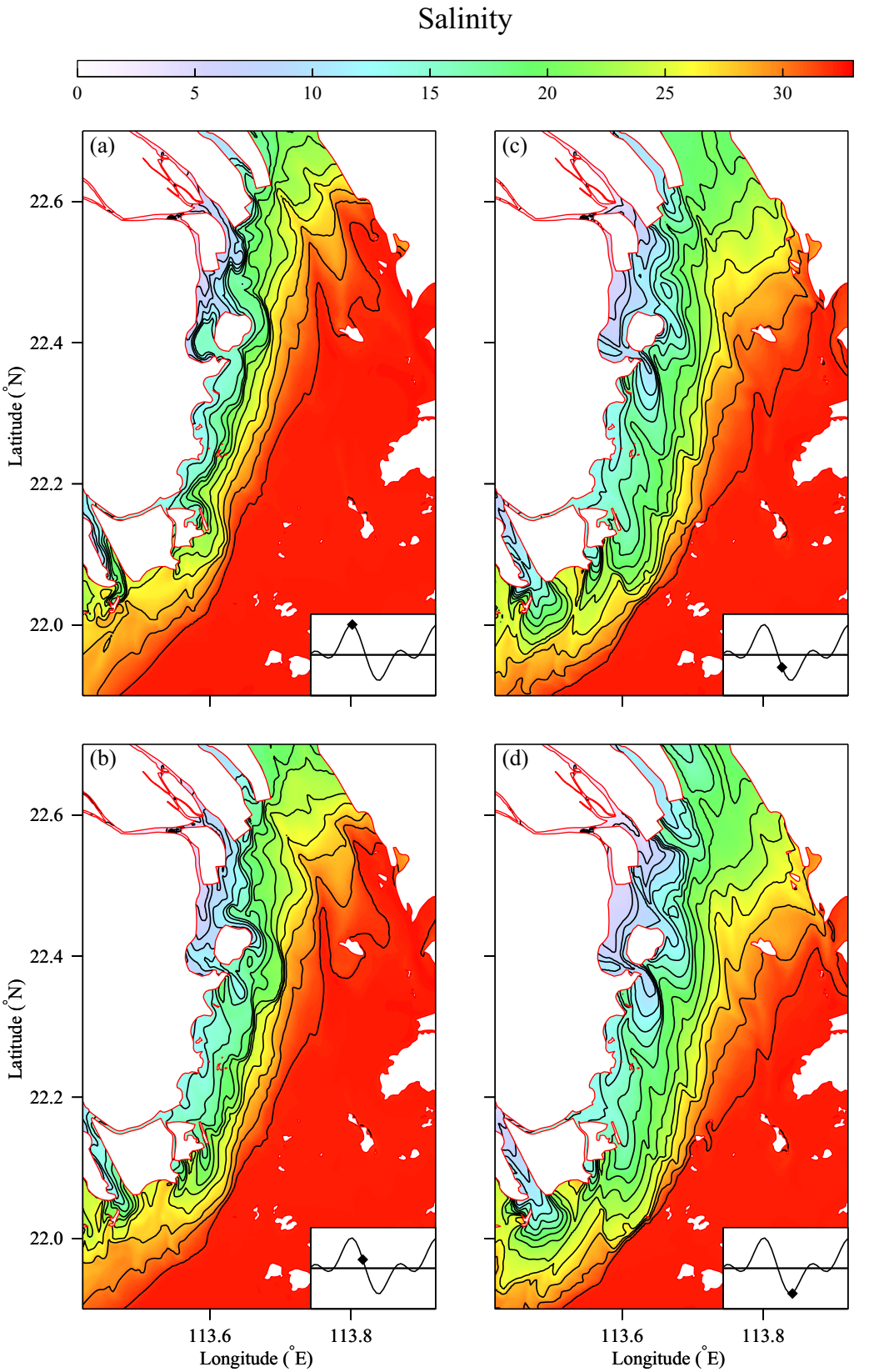

Figure 7. Distributions of the surface salinity in the PRE during the spring tide on 23 GMT, 12 December 2011 (a), 02 (b), 04 (c), and 06 (d) GMT, 13 December 2011, respectively. The salinity contour interval is 2 and the contour line at the southernmost position represents 34.

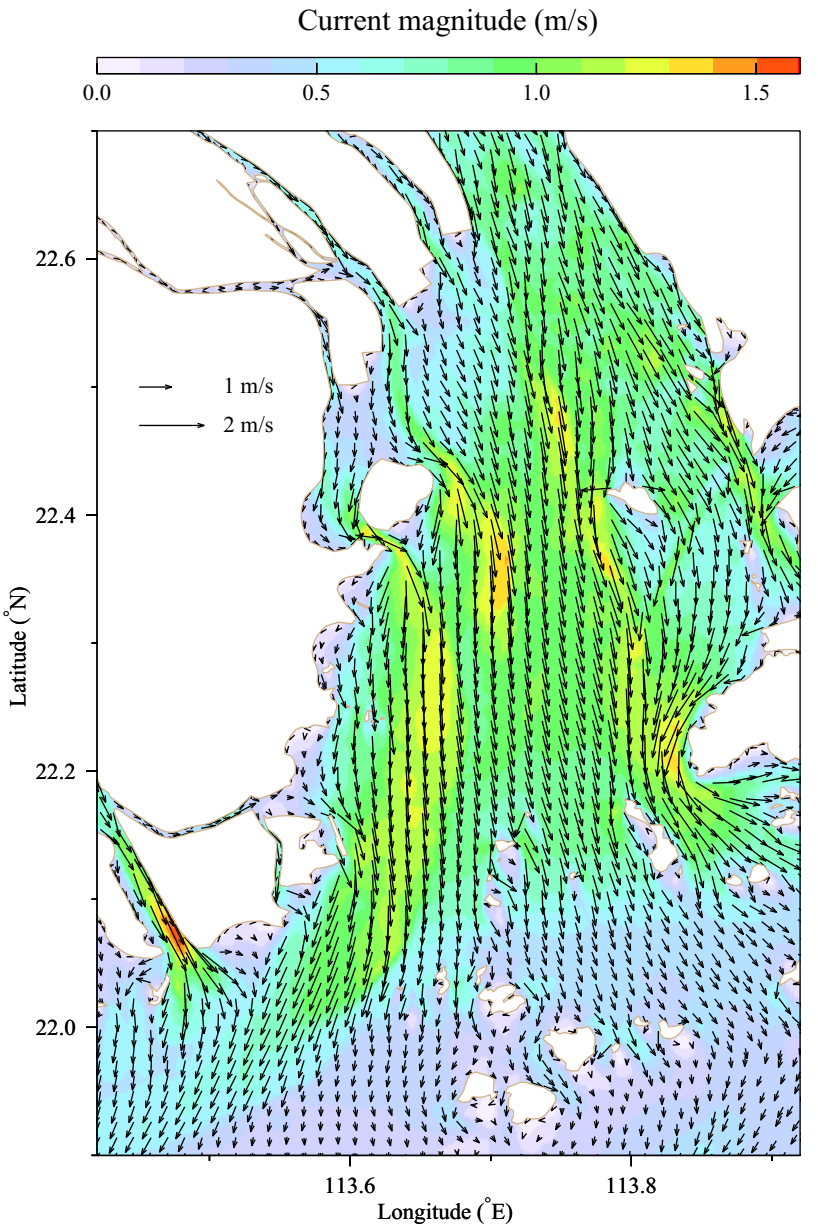

Figure 8. Distribution of the surface currents in the PRE at the same time as that shown in Figure 7c.

The model results show that the riverine plume structure was significantly affected by local geometry (Figures 7b–7d). For example, during the ebb tide, when the riverine plume reached the QiAo Island, it split into two branches. One branch passed by the island on its offshore side and then quickly dispersed into surrounding waters. The other branch flowed through a 1.3 km wide narrow channel between the island and mainland of the delta (hereafter referred to as QiAo Channel). It was this branch of the riverine plume that transported a significant amount of low-salinity water and formed a local discharge plume with a distinct salinity structure over the West Shoal (Figure 7d). To distinguish this local plume with the entire Pearl River plume, we referred it to as the "discharge plume", while the entire Pearl River plume was referred to as the "PR plume" in the following sections.

The QiAo Channel had a strong influence on the PR plume. An example is shown in Figure 8, which displayed the surface current field at the maximum ebb tide (see Figure 7c). This figure shows that the discharge plume was associated with a very strong flow that was concentrating on the course of plume spreading. This dynamical feature resembled the pulse discharge of the tidal plume in the Columbia River

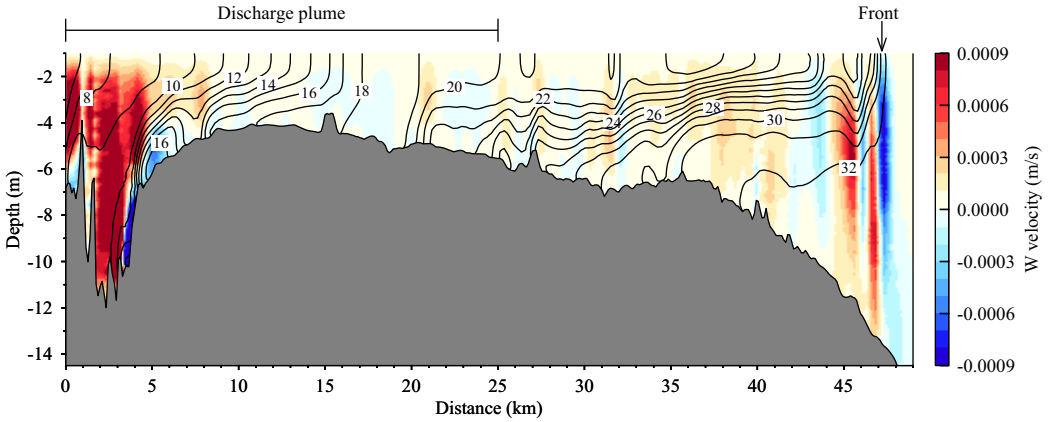

Figure 9. Salinity contours overlapped with vertical velocity image on the transect H4 at the same time as that shown in Figure 7d.

[*Horner-Devine et al*., 2009]. A detailed discussion is given on the dynamics of this geometrically-formed discharge plume in the next section.

4.2. Dynamics of the Discharge Plume

To examine the vertical structure and the evolution of the discharge plume over the West Shoal, a cross-sectional plot along its main axis is shown in Figure 9. Generally, the discharge plume had a longitudinal length scale of ~25 km covering from its source to the near and far-field region [*Garvine*, 1982]. The source region was traditionally considered as the mouth of a river which was close to the origin of buoyant water. In our case, it referred to the QiAo Channel where the discharge plume was initialized. The nearfield started at the mouth of the Channel which was about 4 km off the origin of the figure axis. At that point, the outflow was supercritical and lifted off from the ground to form a surface-intensified buoyant plume with a vertical length scale of ~2 m. A hydraulic jump likely developed about 3 km farther away from the lifted-off point where the flow tended to be blocked and forced to rise. This can be inferred by the locally strong upwelling in that region, suggesting a change of fluid dynamics from supercritical to subcritical. With the presence of the surface plume, the water in the nearfield was strongly stratified during the ebb tide. Mixing in this region was caused by several factors such as winds, tides, and interfacial shear velocity. As a result, the surface-intensified plume deepened gradually in the course of offshore propagation and at a transition from near to far-field. At the mouth of the estuary, the PR plume formed a sharp surface front whose dynamics were affected by the strong outflow of the discharge plume.

A very strong salinity front appeared on the offshore side of the discharge plume. As shown in Figure 10, this frontal feature started from the exit mouth of the QiAo Channel and extended toward the south with a horizontal length scale of ~7 km. In the frontal zone, the salinity difference was ~6. Since the width of the front was approximately 300 m, the estimated salinity gradient in the cross-front direction was equal to 20 per km. In addition, the model results show that the currents in the plume were locally intensified along the front. This was caused as an inertia effect of the flow at the mouth of the Channel where the currents cannot immediately change its direction to be aligned with the ambient current. As a result, the water was piled up along the front and thus produced a higher pressure offshore near the front to force the flow to turn downstream to the right. This model-revealed feature of the discharge plume formed with similar dynamics of a surface-intensified buoyant plume in which the earth rotation can be neglected [*Garvine*, 1982, 1987]. To verify that, we calculated the Kelvin number (K): a key parameter to estimate the importance of the Coriolis acceleration in the momentum balance near the source of the discharge [*Garvine*, 1995]. Here, $K = fL/\sqrt{g'D}$ is defined as the ratio of the discharge scale to the internal Rossby deformation radius, where f is the local Coriolis parameter, L is the characteristic discharge width, D is the layer thickness of the plume at the source, and g' is reduced gravity. Giving $L = 1.3$ km, $D = 2$ m, and the density difference between the ambient and the buoyant fluids as 5.5 kg/m^3 near the source, the estimated $K = 0.24$, a number close to the typical value of small-scale plumes with relatively small effect from rotation that are often observed in the Connecticut River [*OÇDonnell*, 1993]. As suggested by *Garvine* [1995], small-scale discharge

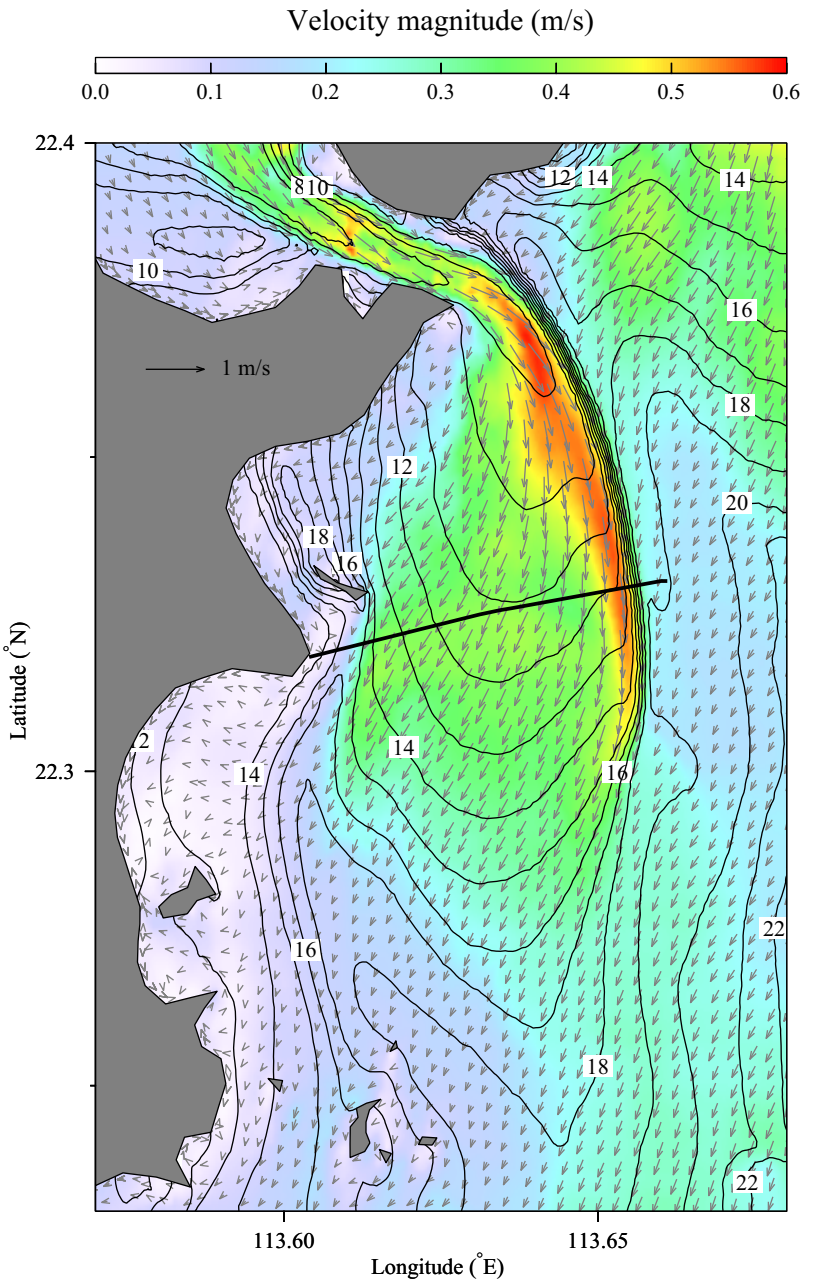

Figure 10. Distributions of the surface currents and salinity of the discharge plume around QiAo Island at the same time as that shown in Figure 7d. The color represents the velocity magnitude at that time. The black line represents the location of the cross-plume transect shown in Figure 12.

usually had relatively fast flow, which made it possible to generate a strong frontal boundary and internal hydraulic jump. These features were confirmed in our results.

4.3. Importance of River Network and Geometric Resolution

The model results suggested that the discharge plume was a major feature of the PR plumes. The geometry of the QiAo Channel and the freshwater passage in the river network were two factors that could significantly influence the plume variability. Specifically, the QiAo Channel featured a very narrow trough with a depth of ~10 m and a channel width of ~1.3 km. This Channel was not resolved in the previous studies for the reason of grid-size limitation. The failure to resolve the geometry of this channel in a model configuration could lead to a wrong or inaccurate water transport of tidal current. In addition, it was clear that a

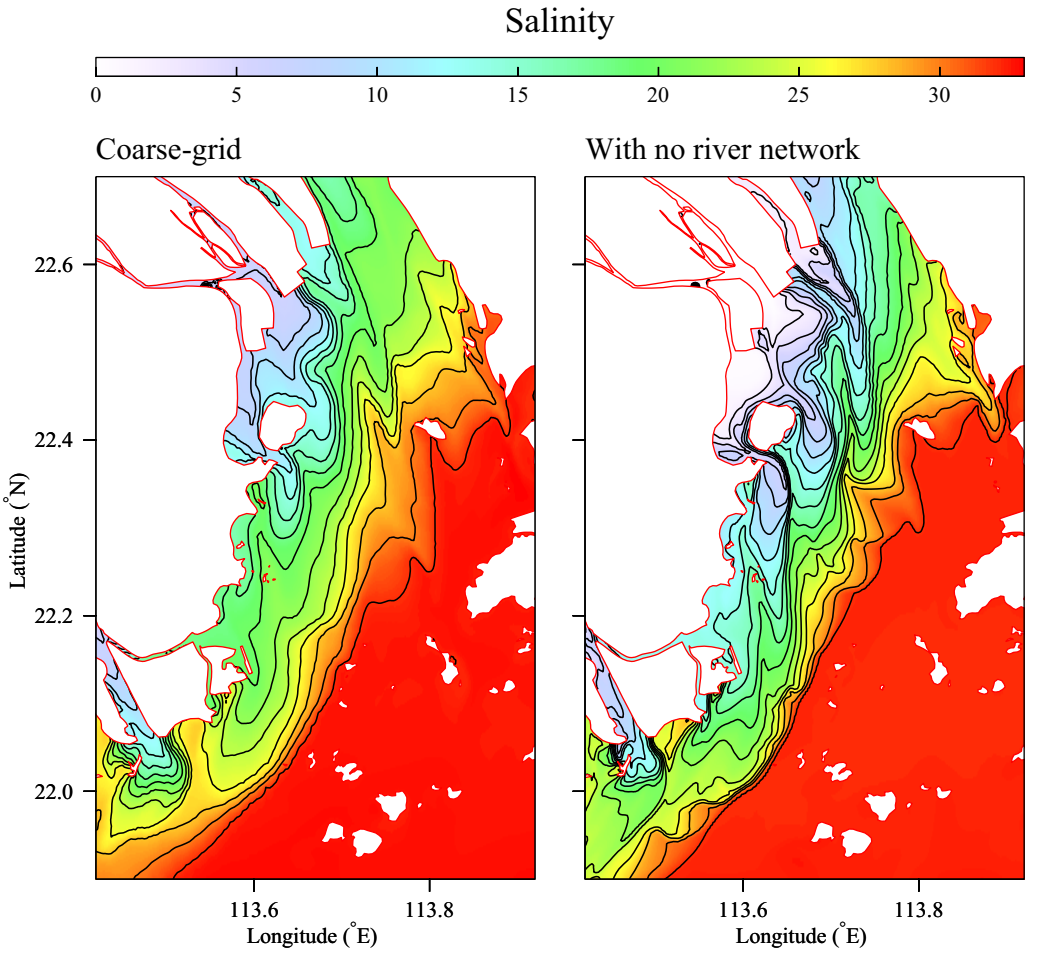

Figure 11. Distributions of the surface salinity in the PRE for the cases with the coarse-grid (left) and exclusion of river network (right) at the same time as that shown in Figure 7d.

portion of freshwater from the upstream river network passed through the Channel during the ebb tide. This part of water transport through the Channel varied significantly as the freshwater discharge through the river network outlets changed and was also affected by the tidal currents in the estuary. So, the amount of the water flowing through the Channel clearly depended on the Channel width, and thus on the model resolution and the freshwater passage in the river network. These can be seen in the following two experiments.

The first experiment was made with the aim at examining the sensitivity of the PR plume to the model resolution. In this experiment, we repeated the model run by reducing the model grid from 130 to 400 m through the Channel and 400–600 m in the estuary. The second experiment was made to evaluate the importance of the river network as freshwater source. In this experiment, we repeated the model run by removing the upstream river network and setting river discharges directly at the locations of the eight river outlets (see Figure 1 for locations), with no change of the total freshwater discharge into the computational domain. The PRE connected the PR network by eight outlets, and the freshwater outflow at an individual outlet was controlled by the integrated dynamical environment in the upstream river network that varied significantly with time. In general, it was extremely difficult to specify accurately the freshwater discharge condition at these eight river outlets. In our experiment, the upstream boundary conditions at individual outlets were specified by distributing the total river discharge (as shown in Figure 3) to each outlet at fixed ratios. These ratios were estimated by the statistical mean weight of the total river discharge at each outlet based on a 9 years measurement from 1999 to 2007 [*Yao et al.*, 2009]. They were 12.1% at Humen; 14.0% at Jiaomen; 13.2% at Hongqimen; 16.2% at Hengmen; 29.6% at Modaomen; 3.7% at Jitimen; 4.9% at Hutiaomen, and 6.3% at Yamen, respectively.

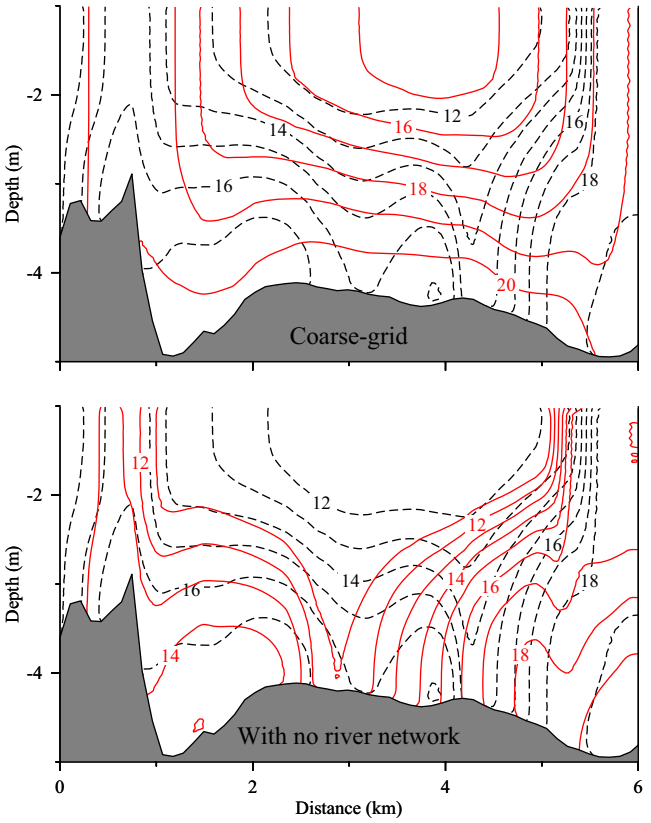

Figure 12. (top) Distributions of the salinity on the cross-plume transect shown in Figure 10 for the cases with the coarse-grid (red) and exclusion of the river network (dashed) at the same time as that shown in Figure 7d. (bottom) Distributions of the salinity on the cross-plume transect shown in Figure 10 for the cases without (red) and with (dashed) the inclusion of the river network at the same time as that shown in Figure 7d.

The results from the first experiment confirmed that the model grid resolution played a critical role in resolving the flow intensity through the QiAo Channel and thus the PR plume. As shown in Figure 11 (left), the coarse grid setup significantly slowed down the channel outflow and thus weakened the discharge plume, a result of an inaccurate fitting of the local coastal geometry. Weakening of the discharge plume had a direct impact on the near-field salinity distribution. In the downstream area of the Channel, the discharge plume became much salter in the coarse grid case (Figure 12, top). This local change had a direct impact on the estuarine-scale salinity distribution. As a result, the PR plume over the West Shoal was also salter and the surface front at the downstream estuarine region was almost invisible. It is evident in Figure 13 (top), which showed that the hydraulic jump found in Figure 9 disappeared in the coarse grid case. In this case, the flow condition changed from supercritical to a Froude number of one or less in the Channel.

The results from the second experiment showed that excluding the upstream river network produced a much larger size plume, and a fresher estuarine condition at the ebb-to-flood transition (Figure11, right). It was clear that ignoring the interaction between the river network and estuary in the upstream area of the Pearl River tended to overestimate the freshwater discharge through the river outlets in the PRE, which can directly enhance the water transport through the Channel and strengthened the discharge plume (Figure 12, bottom). It was also evident in Figure 13 (bottom), which showed that the discharge plume through the QiAo Channel was significantly strengthened and a plume frontal boundary lengthened from the Channel to the downstream estuary with a longitudinal length scale of the discharge plume changing from 25 to 30 km, a 20% increase. Figure 13 also showed that the location of the hydraulic jump shifted about 4 km farther downstream. The water over the West Shoal became completely stratified and the surface front of the PR plume in the downstream estuary significantly intensified.

To verify that the enhanced Channel outflows in the case of excluding the river network was directly linked with the changed freshwater discharges at the river outlets, we compared the freshwater discharge rates specified at outlets for the case excluding the river network with the flux through the outlets simulated in our model for the case including the river network. Specifically, we constructed the time series of the hourly volume flux at individual outlets from the model run and used the 33 h low-passed filter (named PL66) [*Beardsley and Rosenfeld*, 1983] to remove the diurnal and higher-frequency tidal signals from this model data. Then, the 24 h averaging was conducted on the filtered time series to build the daily mean freshwater discharges at each outlet. Following the same approach, we also estimated the daily mean transport through the Channel.

The monthly mean ratios of the freshwater discharges of the eight river outlets for the cases without and with the inclusion of the river network and for the coarse grid case are shown in Figure 14, with a summary

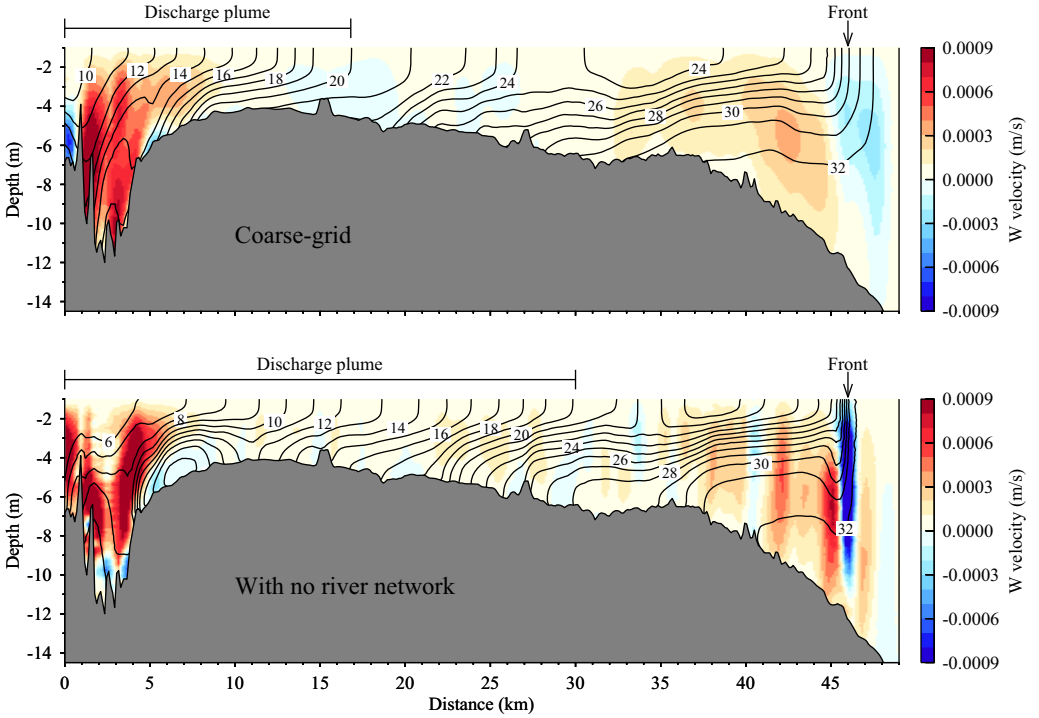

Figure 13. Distributions of the salinity overlapped with vertical velocity image on the cross-plume transect H4 for the cases with the coarse grid (top) and exclusion of the river network (bottom) at the same time as that shown in Figure 7d.

given in Table 3. The daily net water transport through the QiAo Channel for the three cases are shown in Figure 15. Given the same total river discharge rate entering the Pearl River at the upstream end, the amounts and ratios of the freshwater discharges for the cases with and without the inclusion of the river network significantly differed at each outlet (Figure 14 and Table 3). The difference in the discharge rate was up to 17% at Hongqimen and 23% at Hengmen. Consistent with the change of freshwater discharge at the river outlets, the net water transport through the QiAo Channel was much less in the case with the inclusion of the river network than in the case with exclusion of the river network (Figure 15). Excluding the river network accounted for a volume transport increase of 77% through the Channel. This implies that the river network and PRE are a fully coupled dynamical system in which the nonlinear interaction of currents varied significantly with time and in space. Ignoring this interaction process could not only overestimate the freshwater discharge into the PRE but also lead to different ratios of discharge rates at outlets. The change in the amount of the freshwater discharge and discharge rates at each outlet had a direct impact on the plume intensities in the PRE and their spatial and temporal variations. The model results obtained from the case with exclusion of the river network should be interpreted with caution.

It is also interesting to point out here that the impact of the current interaction between the river network and PRE on the freshwater discharges at the river outlets varied with the model resolution. In the coarse-grid case, the total freshwater discharge into the PRE was reduced by a factor of ~6% along with the change in the discharge ratios at the outlets. Correspondingly, the mean water transport through the Channel was reduced by a factor of 30%. This result suggests that it is critical to resolve accurately coastal geometry of the river network if one attempts to get the freshwater discharges at each outlet correct.

5. Discussion

5.1 Dynamics Controlling the River Network and PRE Interactions

The experiments with and without inclusion of the river network suggested that the river network and PRE was a fully coupled nonlinear dynamical system. The question here is: what was the key physical process that controlled the river network and estuary interaction and thus the plume dynamics in this system? Such

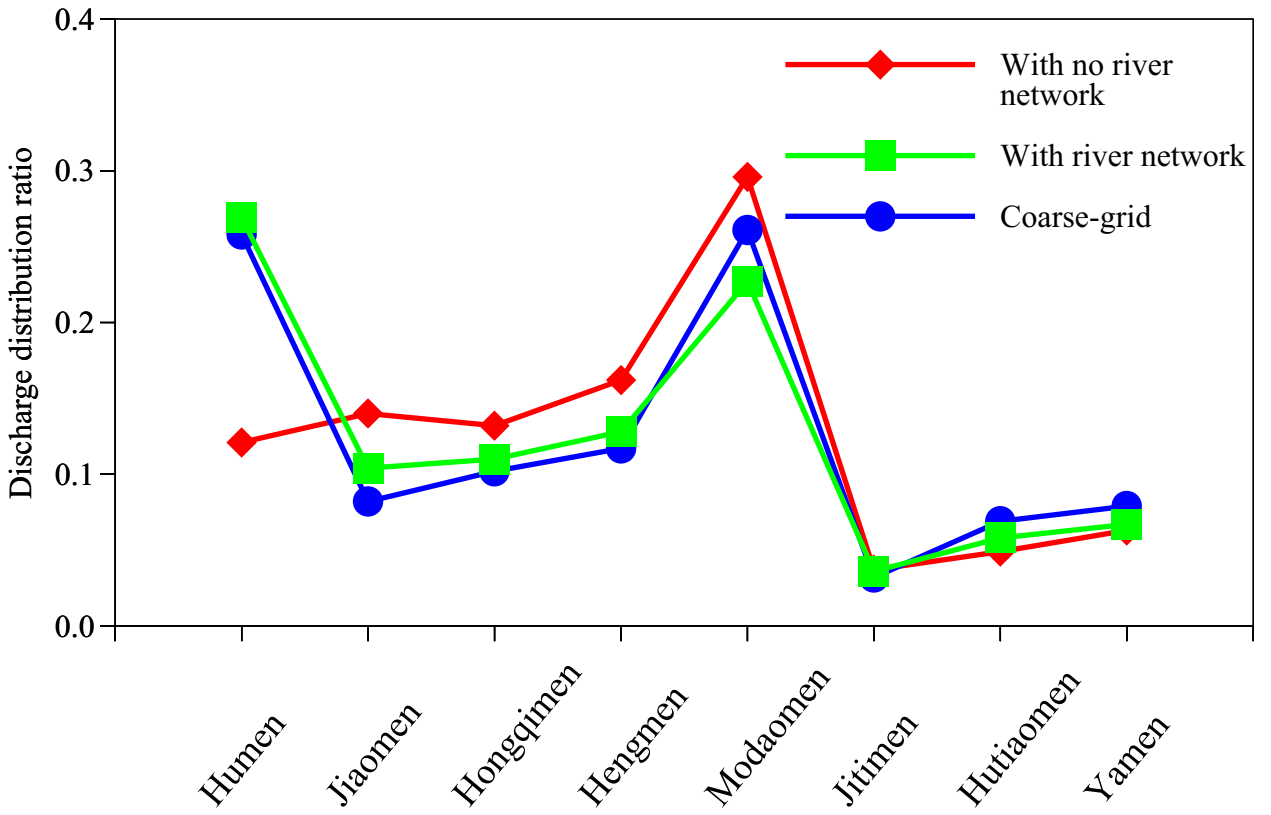

Figure 14. Ratios of freshwater discharge at the eight river outlets for the cases without (red) and with (green) inclusion of the river network and for the case with the coarse grid (blue).

a question is common for a multichannel river plume in an estuary with strong tidal influence, so it was discussed here by providing further insights into the dynamics.

We selected the QiAo Island area as an example to show the complex physical processes contributing to the discharge plume dynamics. As revealed by Figure 15, a persistent pattern of the difference in the net water transport through the QiAo Channel was found over the entire simulation period between the cases with and without inclusion of the river network. This suggests the key physical process should be less sensitive to periodic fluctuation of tidal currents, so we focused our analysis on monthly averaged residual fields. Specifically, the surface residual currents around the QiAo Island in the cases with and without the river network are shown in Figure 16. It suggested that the volume transport through the QiAo Channel was controlled by a very complicated dynamical process which could be explained in the following. On the offshore side of the island, there was a strong seaward current passing by the island in a manner of typical around-island flow. This process was associated with a low pressure center which attached to the island and

Table 3. Mean Freshwater Discharges (Q) and Distribution Ratios (R) at the Eight River Outlets for the Three Cases Listed in the Table[a]

	With the River Network		Without the River Network			Coarse-Grid		
	Q ($m^3 \cdot s^{-1}$)	R (%)	Q ($m^3 \cdot s^{-1}$)	$\triangle Q$ (%)	R (%)	Q ($m^3 \cdot s^{-1}$)	$\triangle Q$ (%)	R (%)
Humen	630	26.9	275	−56.0	12.1	612	−3.0	25.8
Jiaomen	243	10.4	319	31.0	14.0	195	−20.0	8.2
Hongqimen	258	11.0	300	17.0	13.2	243	−6.0	10.2
Hengmen	301	12.8	369	23.0	16.2	279	−7.0	11.7
Modaomen	533	22.7	674	27.0	29.6	620	16.0	26.1
Jitimen	83	3.6	84	1.0	3.7	75	−10.0	3.2
Hutiaomen	136	5.8	112	−18.0	4.9	164	20.0	6.9
Yamen	157	6.7	143	−9.0	6.3	187	19.0	7.9

[a]Note that $\triangle Q$ are the difference relative to the standard case.

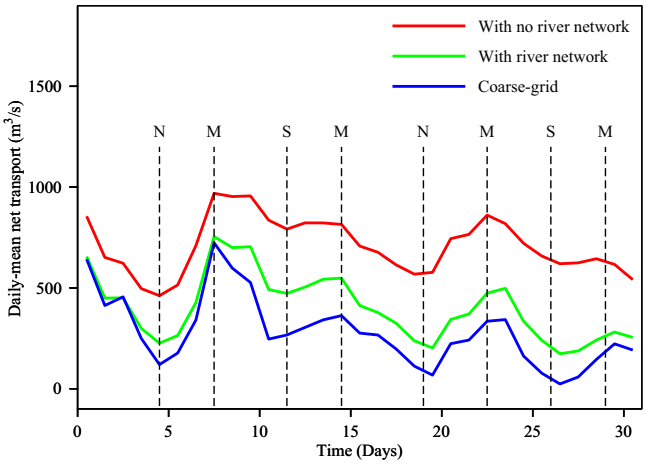

Figure 15. Daily mean net volume transports through QiAo Channel for three cases: red (with no river network), green (with inclusion of the river network), and blue (with the coarse grid) over 1–31 December 2011. Here "M," "N," and "S" represents mean tide, neap tide, and spring tide, respectively.

accelerated the flow by centripetal force. In the case with the river network, the low pressure center was more southward and closer to the Channel. So, it drove a stronger ambient current in the wake of the island. In the case without the river network, however, the low pressure center was more northward and away from the Channel. The resulted ambient current in the wake of the island then became much weaker or even changed the directions to be offshore. When the ambient current met with the outflow near the mouth of the Channel, the frontal process that shown in Figure 10 occurred and generated a higher pressure near the front to against the outflow at the mouth. Since the ambient current in the case without the river network was much weaker than that in the case with the river network, the outflow at the Channel was therefore strengthened significantly.

Clearly, this results suggested the discharge plume dynamics was closely related to the pattern of the strong flow on the offshore side of the island which was further found associated with the SSH in the PRE region. As shown in Figure 17, the difference in the discharge at outlets in these two cases produced significant distributions of the SSH in the upper PRE region connected to the river outlets. In the case with the inclusion of the river network, the contour lines of the residual SSH were primarily in the northeast to southwest direction, which tended to produce a flow to be aligned with the coastline. While, the orientation of the contour lines of the residual SSH turned to the north-south direction in the case with excluding the river network, which intensified the southward flow on the offshore side of the island and thus enhanced the outflow through the QiAo Channel as shown in Figure 16. To verify the connection in dynamics between the estuarine-scale residual SSH field and the discharge plume, one simply can examine the SSH difference shown in Figure 18. By comparing Figure 18 with Figure 15, it clearly showed that the daily variation of the residual flux through the QiAo Channel followed the change of the estuarine-scale SSH difference with zero phase lag. Since a stronger pressure gradient might generate a stronger flow on the offshore side of the island further away from the wake of the island, this could result in a steeper pressure difference at the wake of the island to act against the ambient current

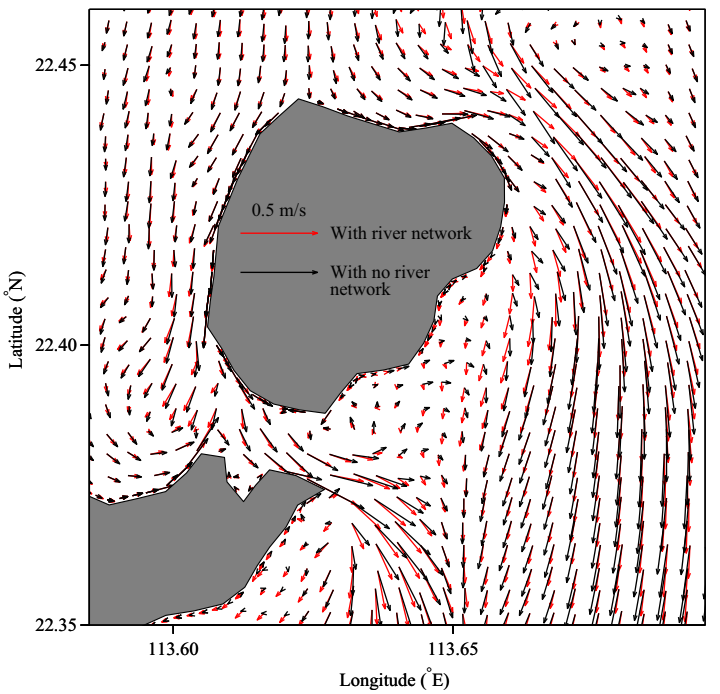

Figure 16. Comparisons of monthly mean residual surface currents for the cases with no river network (black) and inclusion of the river network (red).

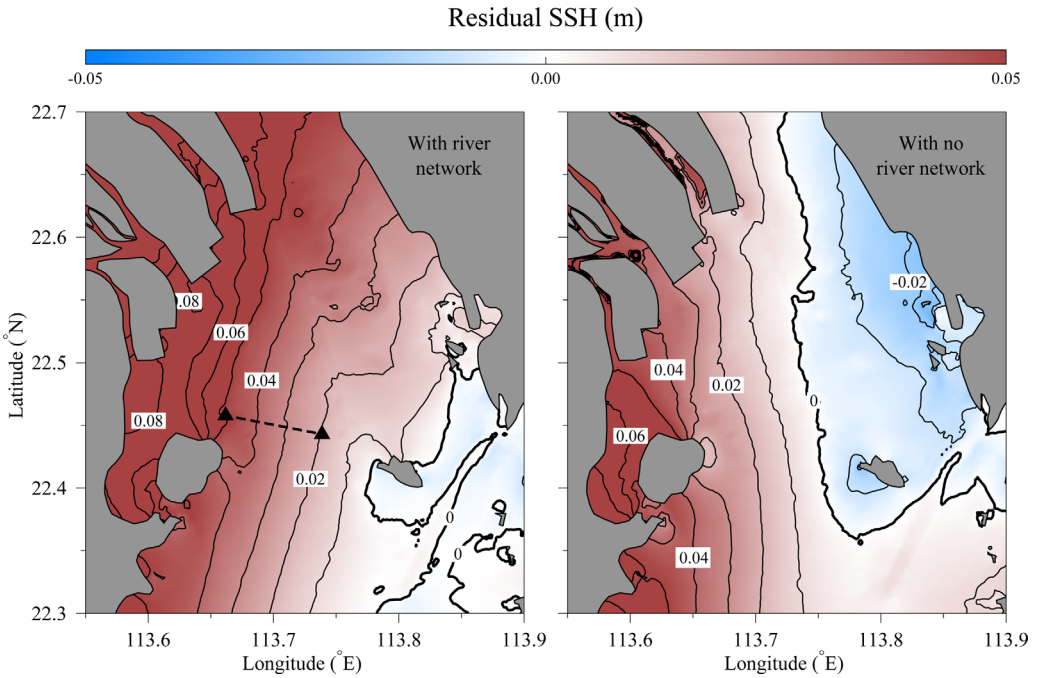

Figure 17. Distributions of the monthly mean residual surface height for the cases with (left) and without (right) inclusion of the river network. The filled triangles connected by a dashed line indicate the locations where the SSH difference was calculated on the offshore side of the QiAo Island.

and weaken the current to a larger degree. This might explain why the estuarine-scale pressure field could interact with such local dynamics around the island and led to a varying outflow through the QiAo Channel.

However, the basic question remained: what caused the shift of the orientation of the estuarine-scale SSH field once the river network was excluded in the model? We believed it was associated with tidal resonance in the PRE. By closing the model domain at the river outlets, it essentially changed the length of the estuary. If that length is about quarter tidal wavelength, then tidal resonance could occur and the enhanced tidal currents could change the estuarine circulation and lead to the shift of the estuarine-scale pressure field [*Knauss*, 1997]. For the PRE, this effect was potentially most significant at the east part of the estuary because the river channel through Humen was the major passage for the tidal energy flux [*Ni et al.*, 2011]. Coincidently, the

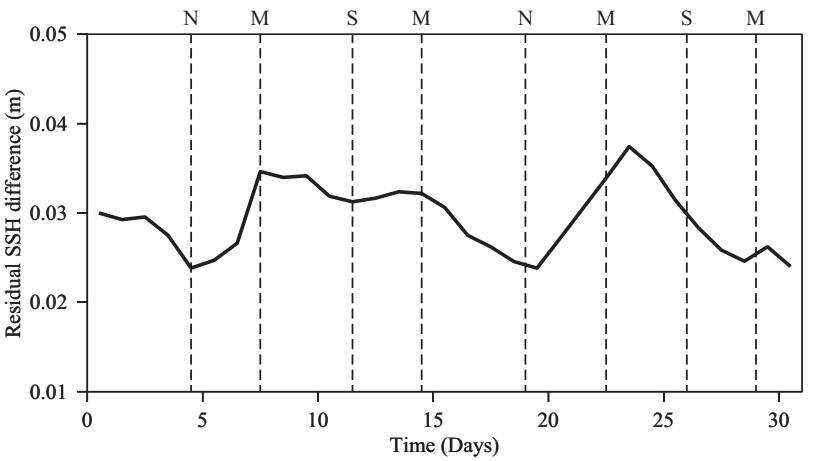

Figure 18. Daily mean surface height difference at the location indicated in Figure 17. The definitions of M, N, and S are the same as those in Figure 15.

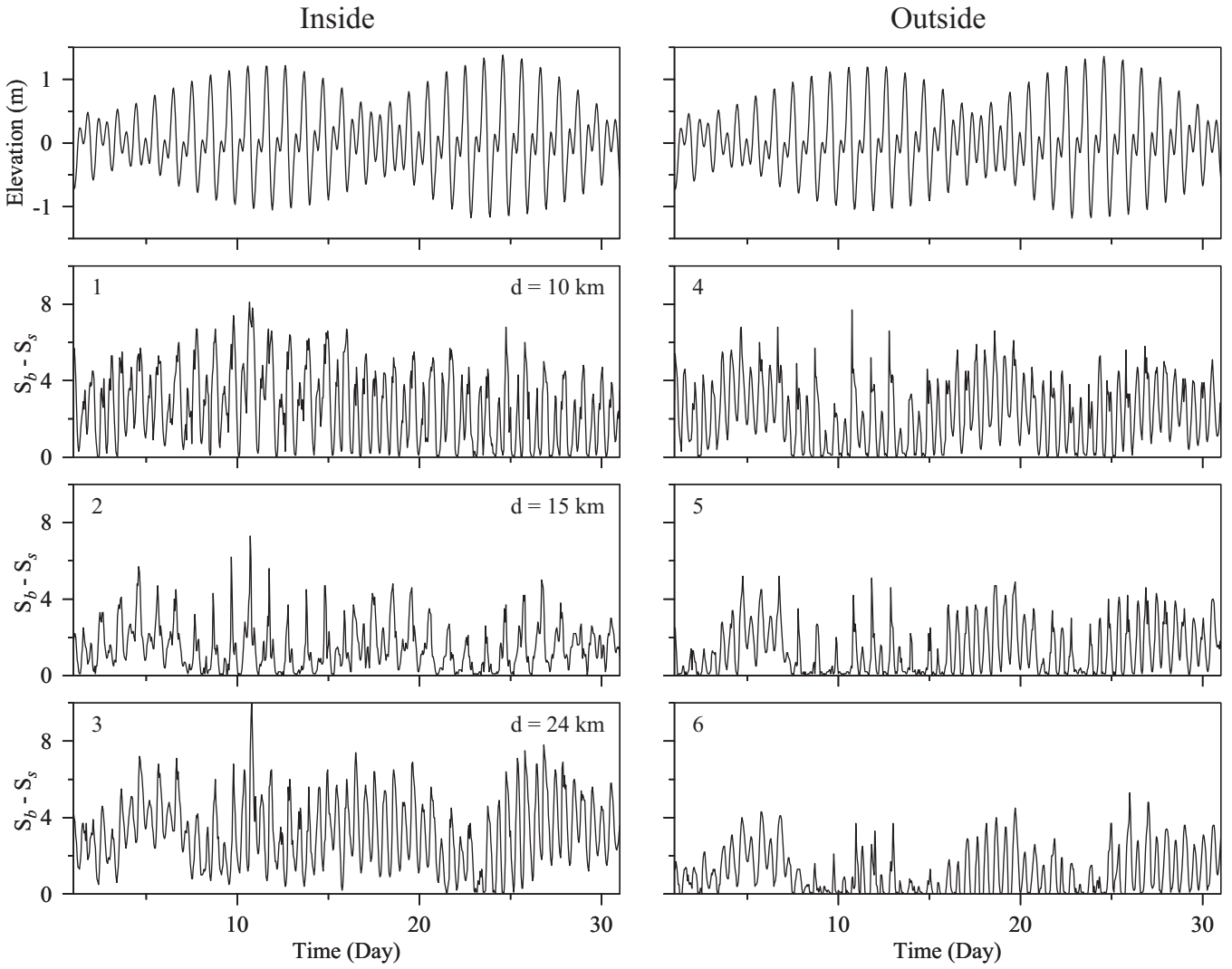

Figure 19. (top) Time series of the surface elevation at station #2 and #5, respectively over 1–31 December 2011. (bottom left) Time series of the surface and bottom salinity difference at station #1, #2, #3, respectively. Label "d" and digital number in each figure indicate the distance relative to the origin defined in Figure 9. (bottom right) Time series of the surface and bottom salinity difference at station #4, #5, #6, respectively. The locations of these stations are marked in Figure 2.

model-predicted SSH field did show a remarkable change in the eastern region of the estuary. We then checked the tidal resonance condition for the case of excluding river network. Assuming that the tide in the PRE was a long gravity wave with a phase speed of $c=\sqrt{gH}$, where c is the wave phase speed, g is the acceleration of gravity, and H is the average depth of the estuary (~5 m for the PRE), the quarter wavelength for the resonance of the semidiurnal tide with a 12 h period was 76 km, which was close to the distance of ~78 km between Humen and the mouth of the estuary. It suggested that tidal resonance could occur in the estuary in the semidiurnal period once the river network was removed with a boundary at Humen. This can be proved by using T_Tide [*Pawlowicz et al.*, 2002] to conduct a harmonic analysis of the surface height time series close to Humen. The results showed that the amplitude of the semidiurnal M_2 and S_2 tidal components could increase by 40% in the case with excluding the river network.

5.2. ROFI of the Discharge Plume

There are a number of studies on small-scale river plumes, with examples in the Connecticut or Merrimack rivers [*Garvine*, 1974, 1987; *O'Donnell*, 1990; *O'Donnell et al.*, 2008; *Hetland and MacDonald*, 2008]. These studies were focused on the frontal features of the plume discharge that were strongly affected by tides. However, less attention was paid to the water column stability in the region of freshwater influence (hereafter referred to as ROFI). In the ROFI of the Rhine River with a feature of strong tidal plume, for

example, the tidal straining due to the interactions of tidal current and horizontal density gradients resulted in the semidiurnal stratification of the water column [*Simpson et al*., 1993; *Simpson and Souza*, 1995; *de Boer et al*., 2006, 2008]. Since the discharge plume is a small-scale feature, it was interesting to see whether the ROFI would exhibit similar dynamics in stratification as found in a typical large-scale river plume.

We examined the monthly time series of the surface and bottom salinity difference at stations #1–#3 in the ROFI of the discharge plume and at stations #4–#6 outside the discharge plume but still within the PR plume (Figures 2 and 19). The results clearly showed that tidal straining had a significant effect on the PR plume, causing the water to be strongly stratified during the ebb tide and vertically well mixed during the flood tide (Figure 19, right). Similar to the Rhine ROFI, the time-dependent switching of water stratification mainly occurred at the semidiurnal tidal period. In the ROFI of the discharge plume, however, the results were different in space. For example, station #1 was about 10 km away from the freshwater source and closer to the Channel exit where the water was strongly influenced by the tidal displacement of the discharge plume and the release of low-salinity water. At this station, the variation of water stratification followed a flood-ebb tidal cycle over a semidiurnal period. This variation was caused by the advection of the discharge plume while the effect of tidal straining was relatively unimportant [*Simpson et al*., 1993]. In contrast, station #2 at 5 km further downstream showed a completely different variation pattern (Figure 19, left) where the dominant switching period changed from semidiurnal to diurnal, which was different from those found in the Rhine River. It seemed this shift was caused as the change of water stratification over the semidiurnal period was suppressed by the plume discharge. At station #3, located at the farthermost edge of the discharge plume, the water remained stratified during most of the simulation period, although the vertical salinity difference varied significantly over semidiurnal tidal cycles.

6. Conclusions

A high-resolution FVCOM-based 3-D circulation model was established for the Pearl River estuary (PRE) and named PRE-FVCOM. PRE-FVCOM integrated the PRE and river network into a coupled dynamics system with accurate resolution of the PRE and coastal geometries. This model was used to study the impacts of the river network on the plume dynamics in the PRE during the dry season. The results showed that the PR plume during the dry season was a distinct feature along the western coast of the estuary. Three types of the plume water masses were identified based on the salinity distribution from the upstream river network to the ambient receiving coastal water. They were (a) riverine water ($<$5), (b) estuarine water ($\sim$12–20), and (c) diluted water ($>$22), respectively. The formation of these three distinct water masses reflected the mixing history of tides and the wind stress in overcoming the initial buoyancy input in the plume.

The model results suggested that this plume was a typical feature of ebb-tide river discharge. When the discharged low-salinity water reached the QiAo Island, the fast flow through the QiAo Channel produced a strong frontal boundary and internal hydraulic jump in a small-scale discharge. The discharge plume formed with similar dynamics of a surface-intensified buoyant plume in which the earth rotation can be neglected due to a small Kelvin number. This feature is similar to the Connecticut River but is different with large scale river plume such as the Rhine or Columbia rivers. This plume had a large impact on the salinity and flow fields over the West Shoal, with its intensity varying significantly as the freshwater discharges at the river network outlets changed.

The model results with and without inclusion of the river network implies that the river network and PRE were a fully coupled dynamical system in which the nonlinear interaction of currents varied significantly in time and space. Ignoring this interaction process could not only overestimate the freshwater discharge into the PRE but also lead to different ratios of discharge rates at outlets. The change in the amount of the total freshwater discharge and discharge rates at each outlet had a direct impact on the plume intensities in the PRE and their spatial and temporal variations. In addition, the distance between Humen and the mouth of the estuary was close to the quarter wavelength of the semidiurnal tidal waves entering the PRE. Truncating the computational domain at the river network outlet in the PRE could lead to a semidiurnal tidal resonance and thus change the tidal dynamics and its impact on the plume in the PRE.

The model results also suggested that inaccurate resolution of the geometric structure in the river network and island complex in the PRE could produce a bias in the amount and distribution ratios of freshwater

discharges at the river network outlets. In the coarse-grid case, the freshwater discharge into the PRE was reduced by a factor of ~6% along with the change in the discharge ratios at the outlets and the water transport through the QiAo Channel could be reduced by a factor of 30%. Therefore, it is critical to resolve accurately coastal geometry of the river network if one attempts to get the freshwater discharges at each outlet correct.

Acknowledgements

We would like to thank Ian S. F. Jones who became deeply involved in discussions during the preparation of the manuscript and provided very constructive comments to strengthen the paper significantly. The research work was supported by the National Natural Science Foundation of China (grant 41206005), the Ocean Public Welfare Scientific Research Project, State Oceanic Administration of the People's Republic of China (grant 201305019-3) and the CAS Strategic Pilot Science and Technology (XDA11020205). Changsheng Chen's participation was supported by the International Center for Marine Studies, Shanghai Ocean University. We would like to thank the Network and Information Technology Center at Sun Yat-Sen University for providing the computing resources. The data used in the paper were accessible by contacting with the authors and depending on the purpose of usage.

References

Beardsley, R. C., and L. K. Rosenfeld (1983), Introduction to the CODE-1 moored array and large-scale data report, in *CODE-1: Moored Array and Large-Scale Data Report*, Tech. Rep. WHOI-*83-23*, *CODE Tech. Rep*. 21, edited by L. K. Rosenfeld, pp. 1−16, Woods Hole Oceanogr. Inst., Woods Hole, Mass.

Chao, S. Y. (1988), Wind-driven motion of estuarine plumes, *J. Phys. Oceanogr.*, *18*(8), 1144–1166.

Chao, S. Y., and W. C. Boicourt (1986), Onset of estuarine plumes, *J. Phys. Oceanogr.*, *16*(12), 2137–2149.

Chen, C. (2000), A modeling study of episodic cross-frontal water transports over the inner shelf of the South Atlantic Bight, *J. Phys. Oceanogr.*, *30*, 1722–1742.

Chen, C., L. Zheng, and J. Blanton (1999), Physical processes controlling the formation, evolution, and perturbation of the low-salinity front in the inner shelf off the Southeastern U.S.: A modeling study, *J. Geophys. Res.*, *104*(C1), 1259–1288.

Chen, C., H. Liu, and R. C. Beardsley (2003), An unstructured, finite-volume, three-dimensional, primitive equation ocean model: Application to coastal ocean and estuaries, *J. Atmos. Oceanic Technol.*, *20*, 159–186, doi:10.1175/1520-0426.

Chen, C., R. C. Beardsley and G. Cowles (2006a), An unstructured grid, finite-volume coastal ocean model (FVCOM) system, *Oceanography*, *19*, 78–89, doi:10.5670/oceanog. 2006.92.

Chen, C., R. C. Beardsley, and G. Cowles (2006b), An unstructured grid, finite-volume coastal ocean model-FVCOM user manual, 2nd ed., *SMAST/UMASSD Tech*. *Rep. 06–0602*, 318 pp., Univ. of Mass.-Dartmouth, New Bedford.

Chen, C., Z. Lai, R. C. Beardsley, Q. Xu, H. Lin, and N. T. Viet (2012), Current separation and upwelling over the southeast shelf of Vietnam in the South China Sea, *J. Geophys. Res.*, *117*, C03033, doi:10.1029/2011JC007150.

Chen, C., et al. (2013), An unstructured-grid, finite-volume community ocean model FVCOM user manual, 3rd ed., *SMAST/UMASSD Tech*. *Rep. 13–0701*, 404 pp., Univ. of Mass.-Dartmouth, New Bedford.

Choi, B. J., and J. L. Wilkin (2007), The effect of wind on the dispersal of the Hudson River plume, *J. Phys. Oceanogr.*, *37*(7), 1878–1897.

de Boer, G. J., J. D. Pietrzak and J. C. Winterwerp (2006), On the vertical structure of the Rhine region of freshwater influence, *Ocean Dyn.*, *56*(3–4), 198–216.

de Boer, G. J., J. D. Pietrzak, and J. C. Winterwerp (2007), SST observations of upwelling induced by tidal straining in the Rhine ROFI, *Cont. Shelf Res.*, *29*(1), 263–277.

de Boer, G. J., J. D. Pietrzak, and J. C. Winterwerp (2008), Using the potential energy anomaly equation to investigate tidal straining and advection of stratification in a region of freshwater influence, *Ocean Modell.*, *22*(1–2), 1–8.

Dong, Z., S. Li, and C. Sheng (1985), Primary analysis of features of residual current in the Pearl River Estuary, *J. Trop. Geogr.*, *5*(3), 177–185.

Dong, L., J. Su, L. Wong, Z. Cao, and J. Chen (2004), Seasonal variation and dynamics of the Pearl River plume, *Cont. Shelf Res.*, *24*(16), 1761–1777.

Fong, D. A., and W. R. Geyer (2001), Response of a river plume during an upwelling favorable wind event, *J. Geophys. Res.*, *106*(C1), 1067–1084.

Fong, D. A., and W. R. Geyer (2002), The alongshore transport of freshwater in a surface-trapped river plume, *J. Phys. Oceanogr.*, *32*(3), 957–972.

Gan, J., L. Li, D. Wang, and X. Guo (2009), Interaction of a river plume with coastal upwelling in the northeastern South China Sea, *Cont. Shelf Res.*, *29*(4), 728–740.

Garcia Berdeal, I., B. M. Hickey, and M. Kawase (2002), Influence of wind stress and ambient flow on a high discharge river plume, *J. Geophys. Res.*, *107*(C9), 3130, doi:10.1029/2001JC000932.

Garvine, R W. (1974), Physical features of the Connecticut River outflow during high discharge, *J. Geophys. Res.*, *79*(6), 831–846.

Garvine, R. W. (1982), A steady state model for buoyant surface plume hydrodynamics in coastal waters, *Tellus*, *34*(3), 293–306.

Garvine, R. W. (1987), Estuary plumes and fronts in shelf waters: A layer model, *J. Phys. Oceanogr.*, *17*(11), 1877–1896.

Garvine, R. W. (1995), A dynamical system for classifying buoyant coastal discharges, *Cont. Shelf Res.*, *15*(13), 1585–1596.

Halverson, M. J., and R. Pawlowicz (2008), Estuarine forcing of a river plume by river flow and tides, *J. Geophys. Res.*, *113*, C09033, doi: 10.1029/2008JC004844.

Harrison, P. J., K. Yin, J. H. W. Lee, J. Gan and H. Liu (2008), Physical-biological coupling in the Pearl River Estuary, *Cont. Shelf Res.*, *28*(12), 1405–1415.

Hetland, R. D. (2005), Relating river plume structure to vertical mixing, *J. Phys. Oceanogr.*, *35*(9), 1667–1688.

Hetland, R. D. (2010), The effects of mixing and spreading on density in near-field river plumes, *Dyn. Atmos. Oceans*, *49*(1), 37–53.

Hetland, R. D., and D. G. MacDonald (2008), Spreading in the near-field Merrimack River plume, *Ocean Modell.*, *21*(1), 12–21.

Horner-Devine, A. R., D. A. Jay, P. M. Orton and E. Y. Spahn (2009), A conceptual model of the strongly tidal Columbia River plume, *J. Mar. Syst.*, *78*(3), 460–475.

Hu, J., and S. Li (2009), Modeling the mass fluxes and transformations of nutrients in the Pearl River Delta, China, *J. Mar. Syst.*, *78*, 146–167.

Ji, X., J. Sheng, L. Tang, D. Liu, and X. Yang (2011), Process study of dry-season circulation in the Pearl River estuary and adjacent coastal waters using a triple-nested coastal circulation model, *Atmos. Ocean*, *49*(2), 138–162.

Knauss, J. A. (1997), *Introduction to Physical Oceanography*, 309 pp., Waveland Press, Long Grove, Ill.

Kourafalou, V. H., L. Y. Oey, J. D. Wang, and T. N. Lee (1996), The fate of river discharge on the continental shelf: 1. Modeling the river plume and the inner shelf coastal current, *J. Geophys. Res.*, *101*(C2), 3415–3434.

Larson, M., R. Bellanca, L. Jönsson, C. Chen and P. Shi (2005), A model of the 3D circulation, salinity distribution, and transport pattern in the Pearl River Estuary, China, *J. Coastal Res.*, *21*(5), 896–908.

MacCready, P., and W. R. Geyer (2010), Advances in estuarine physics, *Annu. Rev. Mar. Sci.*, *2*, 35–58.

Mao, Q., P. Shi, K. Yin, J. Gan, and Y. Qi (2004), Tides and tidal currents in the Pearl River Estuary, *Cont. Shelf Res.*, *24*(16), 1797–1808.

Mellor, G. L., and T. Yamada (1982), Development of a turbulence closure model for geophysical fluid problem, *Rev. Geophys.*, *20*(4), 851–875, doi:10.1029/RG020i004p00851.

Ni, P., X. Wei, C. Wu, and H. Liu (2011), Tidal energy flux and dissipation in the Pearl River estuary, *Ocean Eng.*, *29*(3), 67–75.

Nof, D., and T. Pichevin (2001), The ballooning of outflows, *J. Phys. Oceanogr.*, *31*(10), 3045–3058.
O'Donnell, J. (1990), The formation and fate of a river plume: A numerical model, *J. Phys. Oceanogr.*, *20*(4), 551–569.
O'Donnell, J. (1993), Surface fronts in estuaries: A review, *Estuaries*, *16*(1), 12–39.
O'Donnell, J., S. G. Ackleson and E. R. Levine (2008), On the spatial scales of a river plume, *J. Geophys. Res.*, *113*, C04017, doi:10.1029/2007JC004440.
Otero, P., M. Ruiz-Villarreal, and A. Peliz (2008), Variability of river plumes off Northwest Iberia in response to wind events, *J. Mar. Syst.*, *72*(1), 238–255.
Ou, S., H. Zhang, and D. Wang (2009), Dynamics of the buoyant plume off the Pearl River Estuary in summer, *Environ. Fluid Mech.*, *9*(5), 471–492.
Pan, J., Y. Gu, and D. Wang (2014), Observations and numerical modeling of the Pearl River plume in summer season, *J. Geophys. Res. Oceans*, *119*, 2480–2500, doi:10.1002/2013JC009042.
Pawlowicz, R., R. C. Beardsley, and S. Lentz (2002), Classical tidal harmonic analysis with error analysis in MATLAB using T_TIDE, *Comput. Geosci.*, *28*, 929–937.
Shu, Y., D. Wang, J. Zhu, and S. Peng (2011), The 4-D structure of upwelling and Pearl River plume in the northern South China Sea during summer 2008 revealed by a data assimilation model, *Ocean Modell.*, *36*(3), 228–241.
Simpson, J. H., and A. J. Souza (1995), Semidiurnal switching of stratification in the region of freshwater influence of the Rhine River, *J. Geophys. Res.*, *100*(C4), 7037–7044.
Simpson, J. H., W. G. Bos, F. Schirmer, A. J. Souza, T. P. Rippeth, S. E. Jones, and D. Hydes (1993), Periodic stratification in the Rhine ROFI in the North Sea, *Oceanol. Acta*, *16*(1), 23–32.
Smagorinsky, J. (1963), General circulation experiments with the primitive equations, I. The basic experiment, *Mon. Weather Rev.*, *91*, 99–164, doi:10.1175/15200493.
Tian, X. (1994), Distribution patterns of temperature in Lingding Yang of the Pearl River Estuary, *Trop. Oceanogr.*, *13*(1), 76–80.
Whitney, M. M., and R. W. Garvine (2005), Wind influence on a coastal buoyant outflow, *J. Geophys. Res.*, *110*, C03014, doi:10.1029/2003JC002261.
Wong, L., J. Chen, and L. Dong (2004), A model of the plume front of the Pearl River Estuary, China and adjacent coastal waters in the winter dry season, *Cont. Shelf Res.*, *24*(16), 1779–1795.
Xu, J., Y. Li, and T. Chen (1981), Features of salt water intrusion and salt wedge movements in Lingding Yang, *Trop. Geogr.*, *3*(1), 36–44.
Xue, H., and F. Chai (2001), Coupled physical-biological model for the Pearl River Estuary: A phosphate limited subtropical ecosystem, in *The Proceedings of the Seventh International Conference on Estuarine and Coastal Modelling*, pp. 913–927, Am. Soc. Civ. Eng., N. Y.
Yankovsky, A. E. (2000), The cyclonic turning and propagation of buoyant coastal discharge along the shelf, *J. Mar. Res.*, *58*(4), 585–607.
Yang, G., C. Li, C. Luo, and Z. Ying (1995), *Coastal Geomorphology Dynamics Research and Application*, pp. 243–276, Zhongshan Univ. Press, Guangzhou.
Yao Z., Y. Wang, and A. Li (2009), Primary analysis of water distribution ratio variation in main waterway in Pearl River Delta [in Chinese], *Pearl River*, *2*, 43–51.
Ying, Z., and S. Chen (1983), Mixing features of freshwater and saline water in Neilingding Yang of the Pearl River estuary, *Acta Oceanol. Sin.*, *5*(1), 1–10.
Zhao, H. (1990), *The Evolution of the Pearl River Estuary*, 357 pp., China Ocean Press, Beijing.
Zheng, S., W. Guan, S. Cai, X. Wei, and D. Huang (2014), A model study of the effects of river discharges and interannual variation of winds on the plume front in winter in Pearl River Estuary, *Cont. Shelf Res.*, *73*, 31–40.
Zu, S., H. Shen, H. Lin, and X. Suo (2007), A study on the salt water intrusion in the Pearl River estuary, *Zhujiang Mod. Constr.*, *12*(6), 1–7.